NASA Tech Briefs

National Aeronautics and
Space Administration


Electronic Components and Circuits


Electronic Systems


Physical Sciences


Materials


Computer Programs


Mechanics


Machinery


Fabrication Technology


Mathematics and Information Sciences


Life Sciences

02-01

January 2002

INTRODUCTION

Tech Briefs are short announcements of innovations originating from research and development activities of the National Aeronautics and Space Administration. They emphasize information considered likely to be transferable across industrial, regional, or disciplinary lines and are issued to encourage commercial application.

Availability of NASA Tech Briefs and TSPs

Requests for individual Tech Briefs or for Technical Support Packages (TSPs) announced herein should be addressed to

National Technology Transfer Center
Telephone No. **(800) 678-6882** or via World Wide Web at **www2.nttc.edu/leads/**

Please reference the control numbers appearing at the end of each Tech Brief. Information on NASA's Commercial Technology Team, its documents, and services is also available at the same facility or on the World Wide Web at **www.nctn.hq.nasa.gov**.

Commercial Technology Offices and Patent Counsels are located at NASA field centers to provide technology-transfer access to industrial users. Inquiries can be made by contacting NASA field centers and program offices listed below.

NASA Field Centers and Program Offices

Ames Research Center
Carolina Blake
(650) 604-1754 or
cblake@mail.arc.nasa.gov

Dryden Flight Research Center
Jenny Baer-Riedhart
(661) 276-3689 or
jenny.baer-riedhart@dfrc.nasa.gov

Goddard Space Flight Center
George Alcorn
(301) 286-5810 or
galcorn@gsfc.nasa.gov

Jet Propulsion Laboratory
Merle McKenzie
(818) 354-2577 or
merle.mckenzie@jpl.nasa.gov

Johnson Space Center
Hank Davis
(281) 483-0474 or
henry.l.davis1@jsc.nasa.gov

John F. Kennedy Space Center
Jim Aliberti
(321) 867-6224 or
Jim.Aliberti-1@ksc.nasa.gov

Langley Research Center
Sam Morello
(757) 864-6005 or
s.a.morello@larc.nasa.gov

Glenn Research Center
Larry Viterna
(216) 433-3484 or
cto@grc.nasa.gov

George C. Marshall Space Flight Center
Vernotto C. McMillan
(256) 544-2615 or
vernotto.mcmillan@msfc.nasa.gov

John C. Stennis Space Center
Kirk Sharp
(228) 688-1929 or
technology@ssc.nasa.gov

NASA Program Offices
At NASA Headquarters there are seven major program offices that develop and oversee technology projects of potential interest to industry:

Carl Ray
Small Business Innovation Research Program (SBIR) & Small Business Technology Transfer Program (STTR)
(202) 358-4652 or
cray@mail.hq.nasa.gov

Dr. Robert Norwood
Office of Commercial Technology (Code RW)
(202) 358-2320 or
rnorwood@mail.hq.nasa.gov

John Mankins
Office of Space Flight (Code MP)
(202) 358-4659 or
jmankins@mail.hq.nasa.gov

Terry Hertz
Office of Aero-Space Technology (Code RS)
(202) 358-4636 or
thertz@mail.hq.nasa.gov

Glen Mucklow
Office of Space Sciences (Code SM)
(202) 358-2235 or
gmucklow@mail.hq.nasa.gov

Roger Crouch
Office of Microgravity Science Applications (Code U)
(202) 358-0689 or
rcrouch@hq.nasa.gov

Granville Paules
Office of Mission to Planet Earth (Code Y)
(202) 358-0706 or
gpaules@mtpe.hq.nasa.gov

NASA TechBriefs

National Aeronautics and
Space Administration

January 2002
02-01

4

BLANK PAGE

Electronic Components and Circuits

Hardware, Techniques, and Processes

Books and Reports

BLANK PAGE

Improved Continuity and Short-Circuit Tester

An open or short circuit can be identified immediately.

Langley Research Center, Hampton, Virginia

A relatively simple test circuit immediately and automatically provides indications of (1) the continuity (or the lack thereof) of the wires of a two-wire cable, plus (2) a short circuit (if any) between the wires. In the case of a coaxial cable, one of the wires can be the shield, the other wire, the center conductor.

Some prior cable-testing circuits indicate whether a cable is defective, but do not immediately and automatically indicate whether the defect is a short or an open circuit. Other prior cable-testing circuits fail to indicate which wire is the defective one in the event of an open circuit. Still other prior cable-testing circuits require separate tests for continuity and shorts. Of course, it is possible to test a cable by manual probing with an ohmmeter or a simple continuity checker, but this procedure is cumbersome and is time-consuming in situations in which there are many cables to test. The present cable tester overcomes the limitations of manual probing and of prior cable-testing circuits.

The tester (see figure) is equipped with sockets that mate with the plugs on both ends of a cable to be tested. There can be several such pairs of sockets (e.g., three as shown in the figure), each pair accommodating one of several different types of plugs that may be in use on cables to be tested. The tester contains a pair of batteries, current-limiting resistors, and light-emitting diodes (LEDs); these components are connected such that current flowing along one of the desired or undesired paths through the cable causes one of the LEDs to light up.

As soon as both ends of the cable are plugged into the tester, the cable completes the circuits through the aforementioned components. Then LED 1 lights or does not light up, indicating continuity or discontinuity, respectively, in one wire (the center conductor in the case of a coaxial cable). Similarly, LED 2 does or does not light up, indicating continuity or discontinuity, respectively, in the other wire (the shield in the case of a coaxial cable). If LED 3 lights up, then this is an indication that there exists an undesired current path (a short circuit) between the two wires in the cable.

The circuit also includes a switch and a pair of banana jacks or other convenient auxiliary connectors for testing LEDs or testing external circuits for continuity. If the switch is in "diode check" position, then an LED should light up when connected to the auxiliary terminals with forward polarity and should not light up when connected with reverse polarity: An LED that passes this test is suitable as a replacement for one of the LEDs in this or a similar tester. If the switch is in "continuity check" position and an external circuit is connected to the auxiliary terminals, the illumination or lack of illumination of LED 3 indicates continuity or lack of continuity, respectively, in the external circuit. If nothing is connected to the auxiliary terminals, then for the purpose of testing a cable, the position of the switch does not matter.

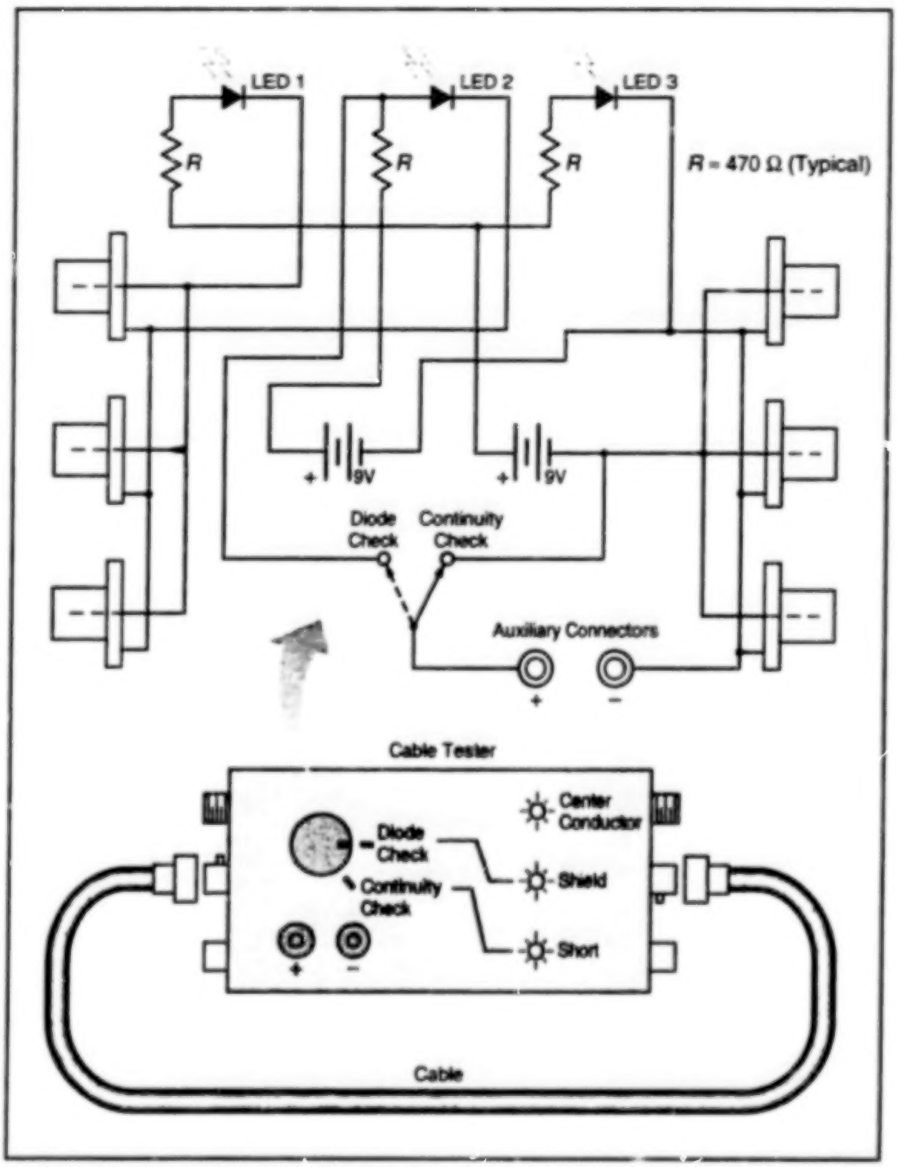

This Cable Tester contains three LEDs that light up to indicate electrical continuity along three paths through a cable connected to a pair of terminals. In addition, an LED or an external circuit can be tested by use of the switch and the auxiliary terminals.

This work was done by Arthur R. Hayhurst of **Langley Research Center**. *Further information is contained in a TSP [see page 1].*

This invention has been patented by NASA (U.S. Patent No. 5,477,152). Inquiries concerning nonexclusive or exclusive license for its commercial development should be addressed to Rheal Turcotte with the NASA Langley Research Center Technology Commercialization Program Office at (757) 864-8881 or r.p.turcotte@larc.nasa.gov. Refer to LAR-14093.

Lateral-Current-Collection HgCdTe Infrared Detectors

Improvements in yield and electrical performance are obtained.

NASA's Jet Propulsion Laboratory, Pasadena, California

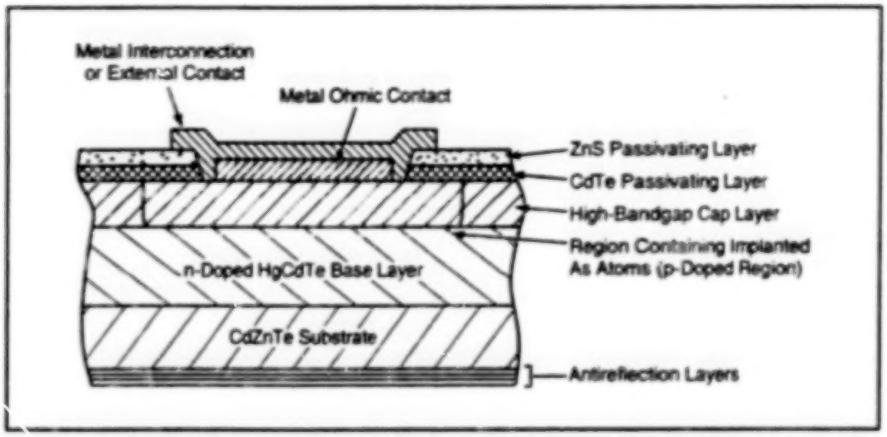

Figure 1. An HgCdTe Photodetector in the Basic DLPH Configuration is fabricated in a process that minimizes contamination.

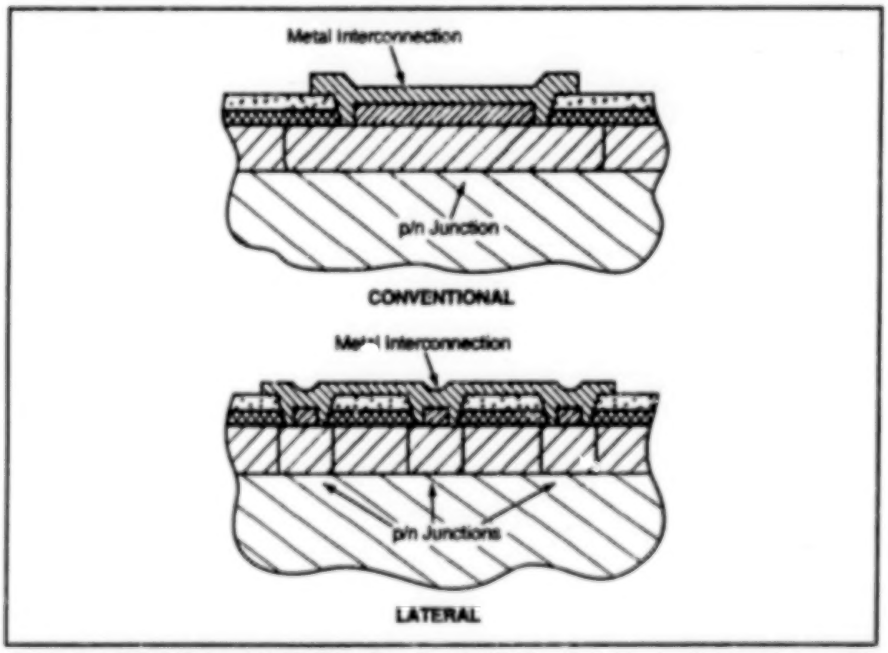

Figure 2. Lateral Current Collection offers the electrical-performance advantages of smaller junction area for a given optical detection area. Decreasing junction area indirectly increases device yield by reducing the probability that a given defect will coincide with a junction.

Arrays of HgCdTe infrared photodetectors have been developed to satisfy stringent performance requirements for use in NASA's Tropospheric Emission Spectrometer. The design of these detectors improves (relative to prior such arrays) manufacturing yield, current-versus-voltage characteristics, and low-temperature performance. The design is of the double-layer planar heterostructure (DLPH) type but differs from conventional DLPH designs in that it features a distinctive lateral current-collection configuration.

Figure 1 depicts the basic DLPH configuration of one of these detectors. An important aspect of the DLPH approach is a planar p-doped/n-doped device geometry that includes a wide-bandgap cap layer over a narrow-bandgap base layer (which is the active device layer). The layers are all initially grown n-doped *in situ* by molecular-beam epitaxy (MBE), thereby ensuring that the critical heterointerface is never exposed to the ambient contamination that has plagued HgCdTe photovoltaic infrared detectors in the past. Then, within the area selected for each detector, arsenic ions are implanted through the cap layer into an upper sublayer of the base layer (which becomes a p-doped sublayer) to form a planar p-on-n photodiode. The implantation step is followed by a two-step thermal anneal in Hg vapor, which is needed to activate the arsenic doping.

A thin passivating layer of polycrystalline CdTe is deposited over the cap layer, then holes for ohmic contacts to the p-on-n diodes are etched in the CdTe, then the ohmic contacts are deposited. The wafer is then overcoated with ZnS, which serves to increase the adhesion of the metal interconnections to be deposited subsequently. Holes are etched in the ZnS to expose the ohmic-contact metal, then the metal interconnections are deposited. Finally, the back side (the lower side in Figure 1) of the wafer is polished and antireflection coated and the wafer is diced into separate detector arrays.

For fabrication as described above, localized defects give rise to area-dependent detector performance, such that conventional DLPH detectors with areas $<10^{-5}$ cm^2 perform considerably better than do detectors with larger areas: this is because reducing the electrical p/n junction area of a diode reduces the probability that a given defect will coincide with the junction. By taking advantage of lateral current collection, which takes place within a few diffusion lengths of a junction, one can obtain, for each detector, a large optically sensitive area with one or more small junction(s). Figure 2 illustrates the difference between the conventional DLPH current-collection configuration and the lateral current-collection configuration.

With proper design, as in the present HgCdTe detector arrays, the optical collection area of a detector can be substantially larger than its electrical junction area. Instead of one diode, each detector pixel contains several diodes formed as small-area implants separated by a distance of the order of one minority-carrier diffusion length and electrically connected in parallel via their ohmic contacts. Following this approach to design and fabrication, optical detection areas can be an order of magnitude greater than electrical junction areas and the advantages of reduced dark current, relatively high resistance, and relatively low capacitance can be realized.

This work was done by Carl Bruce, W. McLevige, and K. Vural of Caltech for **NASA's Jet Propulsion Laboratory**. *Further information is contained in a TSP [see page 1].*

NPO-21002

Real-Time-Programmable Reconfigurable-Vision Active-Pixel Sensors

Images can be subdivided in real-time into overlapping windows with different spatial resolutions.

NASA's Jet Propulsion Laboratory, Pasadena, California

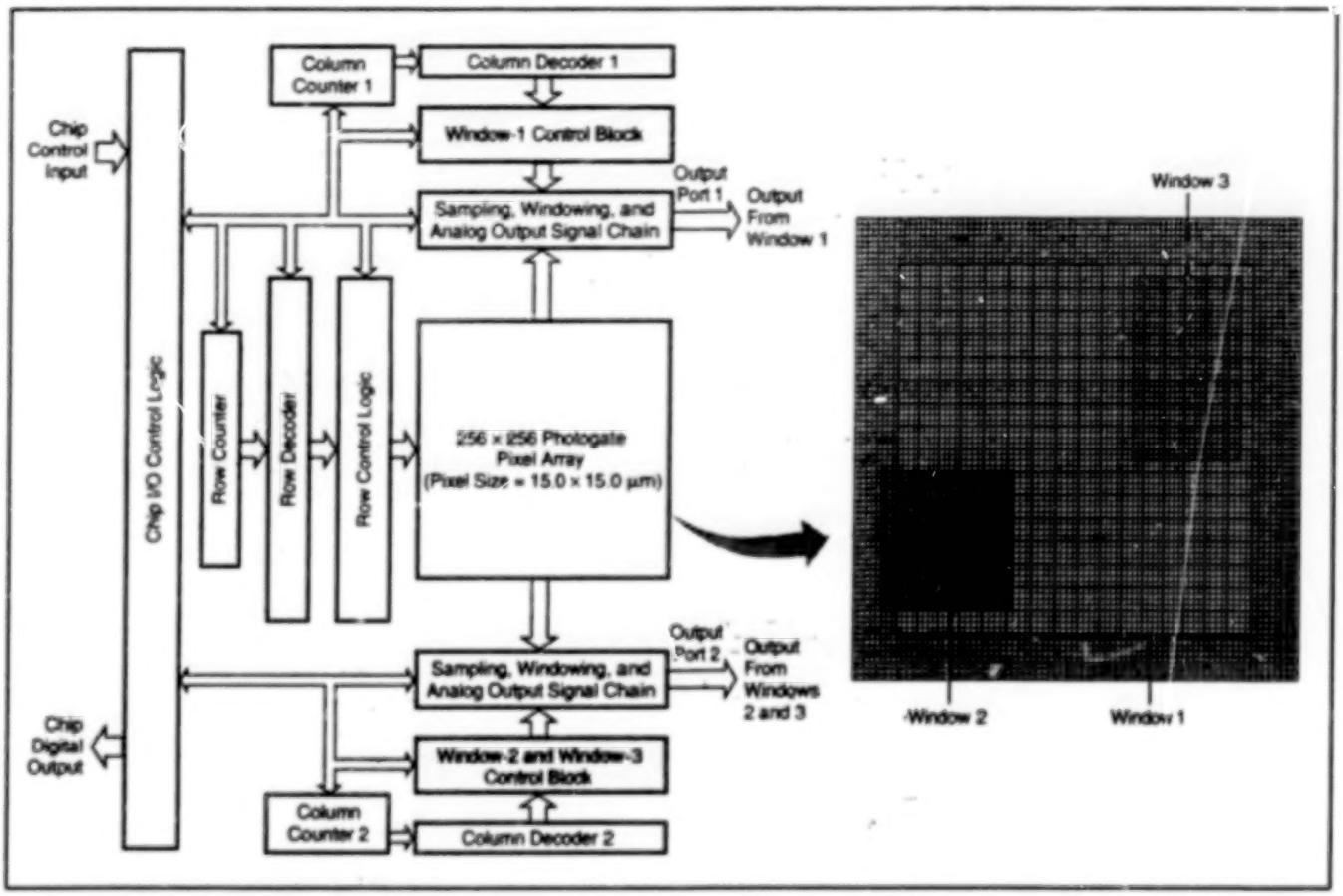

A Prototype Programmable Reconfigurable-Vision Imager contains an array of 256 by 256 pixels. This unit can capture image data from as many as three windows. Window 1 can overlap windows 2 and 3.

Active-pixel integrated-circuit image sensors that can be programmed in real-time to effect artificial reconfigurable vision on demand have been developed and demonstrated. In imitation of a natural eye, the image sensor is designed to offer high resolution in a small region of interest (ROI) within its field-of-view (FOV). In this manner, the imager reduces the amount of unwanted information that must be transferred from the image sensor to external image-data-processing circuitry. Such vision systems are especially attractive for applications that involve recognition of objects and/or tracking of moving targets.

The reconfigurable-vision imager developed at JPL is more powerful than a natural eye or a conventional foveal vision system in the following respects. A conventional foveal vision system is characterized by a number of limitations that have been overcome in the reconfigurable imager:

- The multiresolution lattices are hard-wired; thus, neither ROI location, size, nor the resolution can be changed.
- The multiresolution lattices are typically of a log-polar configuration, which makes them very sensitive to alignment errors and is not compatible with readily available image-data processing algorithms.
- Pixels must be read out serially.
- The high-resolution windows are typically located near the centers of the image frames, effectively restricting their FOVs and requiring mechanical pointing for target acquisition and tracking. Size, power demands, and slow responses of mechanical aiming mechanisms make it difficult or impossible to realize low-power, compact, real-time, active vision systems.

The appropriate resolution for a given ROI is generated using on-focal-plane analog circuits described "Active-Pixel Image Sensors With Programmable Resolution" (NPO-19510), *NASA Tech Briefs*, Vol. 20, no. 5, (May 1996), page 26. Column-parallel arrays of complementary metal oxide semiconductor (CMOS) integrated circuits residing at the bottom of the CMOS pixel array operate simultaneously on the output from a row of pixels to read out of individual pixels or to combine and read the outputs of designated rectangular group of contiguous pixels (superpixels). Unlike the previous work, the reconfigurable imager (see figure) supports multiple ROI, with each ROI independently programmable with respect to size, resolution, and location within the FOV. The imager also consists of a new on-chip digital column-processors to generate and sequence superpixels in real-time. The column-processor features independent and fast reconfiguration of the ROIs in order to provide multiresolution data in real-time. Six control bits per column are needed for each ROI to control the generation of superpixel size, resolution, and location, as well as to sequence the readout of the same. The use of multiple ports and column-processor design allows the imager to simultaneously provide both high- and low-resolution image from the same FOV.

Unlike a traditional foveal vision, the reconfigurable vision system adapts its

acuity profile on a frame-by-frame basis to improve update rates, and to eliminate altogether mechanical gazing. Targets are initially detected in a wide FOV, fast frame rate, and coarse acuity configuration. Following detection, spatial resolution is increased only in the vicinity of the detected objects in order to better resolve targets without wasting system resources on irrelevant scene regions. The coarse-to-fine refinement is analogous to pyramid machine vision techniques, except that the dynamically reconfigurable vision (DRV) system does not require generation of the complete pyramid data structure or the overhead due to high-resolution, wide-FOV, uniform acuity imagery.

This work was done by Bedabrata Pain and Guang Yang of Caltech for **NASA's Jet Propulsion Laboratory**. *Further information is contained in a TSP [see page 1].*

In accordance with Public Law 96-517, the contractor has elected to retain title to this invention. Inquiries concerning rights for its commercial use should be addressed to

Intellectual Property group
JPL
Mail Stop 202-233
4800 Oak Grove Drive
Pasadena, CA 91109
(818) 354-2240

Refer to NPO-20866, volume and number of this NASA Tech Briefs issue, and the page number.

Books and Reports

PWM and Synchronous Rectifier Controller ASICs

A report describes two radiation-hard application-specific integrated circuits (ASICs) that constitute a mixed-signal chip set that performs all the control functions for a power-converter module (PCM) in a spacecraft power-supply system. One of these ASICs serves mainly as a pulse-width modulation (PWM) controller for the circuitry on the primary side of a transformer in the module; the other ASIC is mainly a synchronous rectifier controller (SRC) for the circuitry on the secondary side of the transformer. Both ASICs contain input/output circuits, voltage regulators, power-on reset circuits, and amplifiers for driving complementary heterostructure field-effect transistors (CHFETs). In addition, the PWM ASIC includes a fault monitor, an isolation amplifier, and an error amplifier, through which the pulse width is controlled in response to an error signal generated by the PCM. The SRC ASIC includes a telemetry amplifier, voltage comparators, a high-voltage amplifier, error amplifiers capable of driving the isolation amplifier in the PWM ASIC, and amplifiers for sensing the PCM output voltage and for sensing currents.

This work was done by Barbara Lam, Clint Kwa, David Zhu, Gene Wester, Gregory Carr, John Bennett, Lauro Franco, David Hogue, Pete Skelly, and Russ Haskell of Caltech for **NASA's Jet Propulsion Laboratory**. *To obtain a copy of the report, "Pulse Width Modulator and Synchronous Rectifier Controller ASIC," see TSP's [page 1].*

NPO-30281

Electronic Systems

Hardware, Techniques, and Processes

BLANK PAGE

Hardware and Software for Air-to-Air Schlieren Imaging

Accurate positioning and camera control are necessary for success in schlieren imaging.

Dryden Flight Research Center, Edwards, California

Figure 1. This is a **Ground-to-Air Schlieren Image** of a T-38 airplane. The air-to-air schlieren images are expected to have resolutions of about 1 in. (~2.5 cm).

Software and electronic hardware are being developed to provide cockpit guidance and camera control for an air-to-air schlieren photography system that is to be used to take high-resolution pictures of shock waves generated by a full-scale airplane (see Figure 1). For success in schlieren imaging, it will be necessary to position two airplanes — an observing airplane and the one generating the shock waves — precisely along a line of sight to the Sun, which will be used for illumination. The shock-wave-generating airplane will fly at supersonic speed, while the observing airplane will have to fly at a much lower speed of 250 knots (129 m/s).

The schlieren images will be captured by a charge-coupled-device time-delay integration (TDI) camera. Global Positioning System (GPS) receivers are mounted in both airplanes. The schlieren calculations will be performed by a personal computer with dimensions of about 5 by 8 by 8 in. (about 13 by 20 by 20 cm), ruggedized to withstand acceleration of as much as 5.4 g's.

A two-seat F-18 airplane has been configured for performing the observations. The schlieren computer is located in the rear cockpit. The schlieren camera and its optics are housed in a forward-looking infrared (FLIR) pod. Six-in. (15-cm) monitors are mounted in both cockpits. The computer is equipped with a frame-grabber board and runs Windows NT, Matlab, and Extended Real Time Toolbox software plus the XLA® imaging software.

In addition to positioning of both airplanes precisely, it will be necessary to generate accurate line-scan-rate information, based on the relative positions and velocities of the airplanes and orientations of the airplanes relative to the Sun, to prevent blurring of the schlieren images. Matlab-based software was developed to compute the positions, velocities, orientations, and the corresponding required line-scan rates from the GPS data. The software will display trajectory-guidance information to the pilot of the observing airplane (see Figure 2), will control the operation of the camera, and will cause all trajectory and image data to be recorded in the computer.

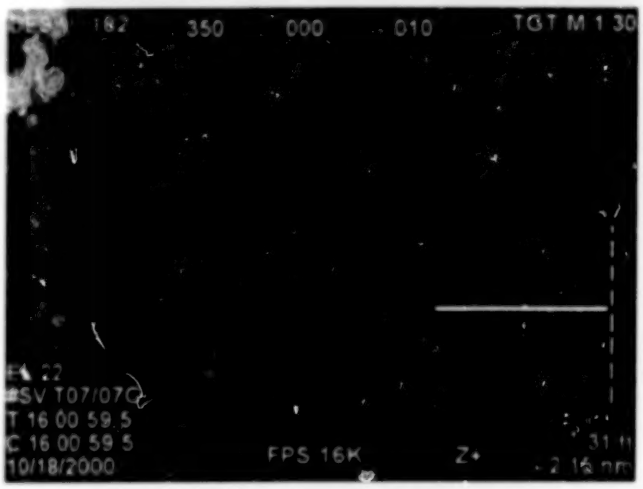

Moving Pilot-Guidance Map

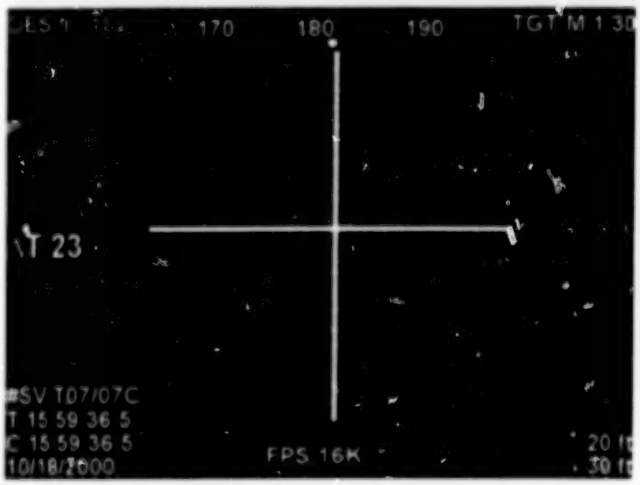

Terminal Pilot-Guidance Needles

Figure 2. A **Moving Map and a Terminal Needle Display** will guide the pilot in positioning the observing airplane to acquire schlieren images.

A moving map showing both airplanes, local landmarks, and restricted airspaces will guide the F-18 pilot in following a trajectory needed for acquiring a schlieren image. This map display includes a scrolling heading indication of the actual and desired headings of both airplanes. Inset guidance needles shows the offset to the required flight track and indicates the required bank angle to capture the track from the downwind leg. The rear-seat operator can select different flight-path separations and map scaling via a graphical user interface or by pressing keys.

When the airplanes are close to the relative position needed for imaging, the display changes to large terminal pilot-guidance needles and includes a time-to-go indication. When the imaging position is reached, the software commands the camera to scan at the proper rate and saves the image in a nonvolatile memory. The operator can also manually command the acquisition of

an image via a graphical user interface or by pressing a key. The schlieren image is displayed to the pilot a few seconds after it is taken. All GPS data from both airplanes are saved for postflight analysis.

The use of commercial off-the-shelf software and hardware for importation of data, generation of graphical displays, and controlling the camera has reduced the time and cost of development of the air-to-air schlieren system. Most of the algorithms implemented in the schlieren software were adapted from code developed previously in-house. In tests of parts of this system on two moving ground vehicles, it was found that positions could be determined accurately to within about 2 ft (≈0.6 m), the system operated with a latency of about 0.3 second, and the TDI camera could be commanded properly. The capability of this system for determining relative positions and providing guidance to the pilot may be used on other flight projects at Dryden Flight Research Center. The Autonomous Formation Flight program will use the relative-position software from the schlieren program as a basis for an independent measurement of relative position.

This work was done by Edward A. Haering, Jr., and David Richwine of **Dryden Flight Research Center**.

DRC-01-38

Portable Airborne Multispectral-Imaging System

This system can be put into operation almost anywhere on short notice.

Stennis Space Center, Mississippi

A Small, Unpiloted, Remotely Controlled Airplane carries video cameras and associated equipment. Terrain images in three spectral bands, plus time and information for registering the images with geographic coordinates, are transmitted from the airplane to a ground-based subsystem during operation.

A portable instrumentation system that includes an airborne and a ground-based subsystem acquires multispectral image data over swaths of terrain ranging in width from about 1/2 to 1 km. The system was developed especially for use in surveying coastal environments; it is also well suited for performing remote sensing in connection with agriculture, aquaculture, forestry, environmental decontamination, and general environmental monitoring. The system can be stowed in two suitcase-size containers that can be transported as check-in luggage on a commercial airline. Once the system has been delivered to its destination and unstowed, the airborne subsystem can be launched over unprepared terrain and controlled from the ground-based subsystem, which can be operated from a minivan or a similarly sized vehicle.

The airborne subsystem includes a small, unpiloted, remotely controlled airplane (see figure) that carries a color forward-looking video camera for navigation, three downward-looking monochrome video cameras for imaging terrain in three spectral bands, a video transmitter, and a Global Positioning System (GPS) receiver. An interference band-pass filter for one of the three spectral bands is mounted in front of the lens of each downward-looking camera. The filters can be changed in the field. The bands, each 10 nm wide, can range in wavelength from 400 to 1,100 nm. The outputs of the four cameras are multiplexed for real-time transmission so that the single video transmitter suffices for sending the image data to the ground station for real-time monitoring and recording; this aspect of the design reduces the cost and weight below what they would otherwise be.

The airplane carries an attitude reference sensor that measures absolute heading, roll, and pitch. This sensor comprises a three-axis magnetometer and a two-axis electrolytic clinometer. The position and reference data acquired by the GPS receiver and the attitude reference sensor can be used to register the multispectral image data with geographical coordinates, without need for predetermined ground reference targets.

The multiplexing of camera outputs is synchronized with, and performed in conjunction with, other functions that include triggering of the cameras, reading and storage of data from the GPS receiver and the attitude reference sensor, and the overlay of time, position, and attitude information on the image data. These functions are performed by a circuit that includes five microcontrollers, a video multiplexer, and a video synchronization separator, all mounted on a prototype circuit board.

The ground subsystem includes a receiver for video and digital data signals, a laptop computer that displays a moving map, a digital video cassette recorder, and a monitor that displays the video images in real time. Both the airborne and the ground subsystems were constructed mostly from commercial off-the-shelf components. Most of the development effort was expended on the airborne subsystem because of the need for miniaturization, minimization of weight, and minimization of the effects of airplane-engine vibrations.

This work was done by Robert Lahnemann and Todd McNamee of Air-O-Space International, LLC for **Stennis Space Center**.

Inquiries concerning rights for the commercial use of this invention should be addressed to the Intellectual Property Manager, Stennis Space Center [see page 1]. Refer to SSC-00089.

Lossless Image-Compression Algorithm Implemented in an FPGA

Compression performance is somewhat better than that of a prior algorithm.

NASA's Jet Propulsion Laboratory, Pasadena, California

A lossless image-compression algorithm that can be executed entirely in electronic hardware has been developed. This algorithm yields about 15 percent more compression than does the Rice algorithm, which is a lossless-compression algorithm commonly used for transmitting images from spacecraft to Earth. A prototype of the hardware (see figure), consisting mainly of a field-programmable gate array (FPGA) and a small random-access memory, has been built and verified to function as intended.

The present algorithm is called "FPGA LOCO" because of the FPGA implementation and because it is a modified version of a prior lossless image-compression algorithm called "Low Complexity Lossless Compression for Images" (LOCO-I). The purpose and effect of the modifications were to reduce the complexity of implementation in hardware and, especially, implementation in an FPGA.

The FPGA LOCO algorithm accepts, as input, a stream of 8-bit data that represent the brightnesses of pixels in a rectangular image. The output of the algorithm is a sequence of bits from which the original image data can be reconstructed.

The FPGA LOCO algorithm is based on the concept of predictive compression. During compression, the pixel data are processed in raster-scan order: Scanning starts at the upper left corner of each image, and pixel positions are incremented along each row before dropping down to the next row. The first two pixels in the first row are simply put into the output bit stream uncoded. For all other pixels of the image, the processing can be considered to be divided into the following steps:

1. Classify the current pixel into one of several contexts according to the values of a small number (usually 5) of previously encoded nearby pixels.
2. Estimate the value for the current pixel by extrapolation from a small number (usually 3) of previously encoded nearby pixels and add a correction (called the bias) that depends on the context.
3. Map the difference between the estimated and actual values of the current pixel to a nonnegative integer, and encode this integer by use of a Golomb code (Golomb codes are relatively simple, variable-length, entropy codes that are well suited for encoding quantities with distributions that are approximately geometric).
4. Update the statistics for the context on the basis of the value for the current pixel.

The prototype hardware (see figure) includes a commercial FPGA installed on a commercial circuit board that features a PC/104 interface. [PC/104 is an industry standard for compact, stackable modules that are fully compatible (in architecture, hardware, and software) with personal-computer data- and power-bus circuitry.] An optional 256K × 18 zero-bus-turnaround (ZBT) static random-access memory (SRAM) is installed on the board with the FPGA. An adaptor card is used as an additional interface between the PC/104 interface and the Industry Standard Architecture (ISA) interface of the computer in which the prototype hardware is installed. To enable simultaneous access to all the data for a context, a second, identical SRAM was installed on a daughter card that is connected to the board via two ribbon cables.

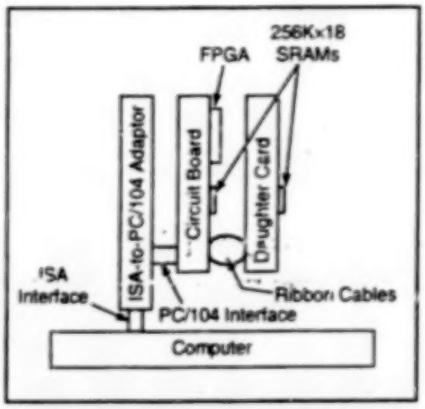

The Prototype Image-Compression Hardware is installed in a computer that supplies the input image data and accepts the output (compressed) image data.

In tests at a clock speed of 12 MHz, the prototype hardware was found to process image data at a rate of 260 kilopixels per second. However, most of the processing time was spent waiting for transfers of data to and from the computer. The throughput rate of the prototype hardware by itself is about 1.33 megapixels per second.

This work was done by Matthew Klimesh, Valerie Stanton, and David Watola of Caltech for **NASA's Jet Propulsion Laboratory**. *Further information is contained in a TSP [see page 1].*

In accordance with Public Law 96-517, the contractor has elected to retain title to this invention. Inquiries concerning rights for its commercial use should be addressed to

Intellectual Property group
JPL
Mail Stop 202-233
4800 Oak Grove Drive
Pasadena, CA 91109
(818) 354-2240

Refer to NPO-21238, volume and number of this NASA Tech Briefs *issue, and the page number.*

High-Performance Processor of Hyperspectral Images

Efficient algorithms analyze pixel spectra to estimate abundances of materials.

Stennis Space Center, Mississippi

The Remote Sensing Hyperspectral Engine (RSHE) is a special-purpose, portable computer that performs high-performance processing of hyperspectral image data collected by a remote-sensing optoelectronic apparatus. Typically, the remote-sensing apparatus is airborne or spaceborne, the images are of terrain, and the purpose of collecting and analyzing the image data is to estimate the spatially varying abundances of materials of interest. Remote-sensing applications in which the RSHE could prove beneficial include assessment of crops, exploration for minerals, identification of military targets, urban-planning studies, environmental assessment, and large-area search-and-rescue operations.

This system is designed to perform the overall functions of (1) extracting a spectral signature of each pixel from the data for a given image and (2) processing the spectral signatures of the pixels to unmix the superimposed spectra of different materials and thereby obtain estimates of the abundances of materials in each pixel of the image. What distinguishes this system

from other such systems are the specifics of its implementation in hardware and software. The hardware comprises mostly commercial off-the-shelf modules and assemblies chosen to afford the required computational capabilities while fitting in an ultracompact package. The most notable aspect of this system is software that processes hyperspectral image data robustly and efficiently and provides enhanced means for displaying and otherwise using the results of processing to facilitate understanding of images.

The software performs so many advanced functions that it must suffice to list only a few of them here:

- The hyperspectral image data are processed by using a Universal Robust Filtering (URF) Software Package (a commercial product developed by the American GNC Corp.) coupled with an optimization algorithm to iteratively search through the space of candidate solutions. Because an optimization algorithm that starts from a tabula rasa involves many iterations and thus is inherently time-consuming, this system takes advantage of the existing correlation between neighboring pixels to reduce the amount of search needed. After obtaining the solution for the first pixel by using the optimization algorithm, the solutions for the rest of the pixels are derived from the computationally efficient robust filtering algorithm.
- The robust nonlinear spatial filter includes the applicable measurement equations and an extended Kalman filter. Constraints on the abundances of the materials of interest, expressed through mathematical models, are incorporated into the filter. Thus, the abundance-unmixing problem is transformed into an augmented, nonlinear filtering problem that is solvable by use of nonlinear, extended Kalman filtering techniques.
- Each material of interest is represented in a reference library of spectral signatures that have been processed into orthonormal basis vectors.
- Identification of materials of interest involves the use of a fuzzy neural network to correlate preprocessed hyperspectral image data with orthonormal reference-signature vectors.
- The graphical user interface facilitates the initiation of processing, retrieval of images, and display of image data. For example, one can choose *N* monochrome two-dimensional displays for *N* materials of interest; the brightness of each pixel of one of the images is an indication of the abundance of the material in question at the pixel location.

This work was done by American GNC Corp. for **Stennis Space Center**.

In accordance with Public Law 96-517, the contractor has elected to retain title to this invention. Inquiries concerning rights for its commercial use should be addressed to

American GNC Corp.
888 Easy Street
Simi Valley, CA 93065

Refer to SSC-00138, volume and number of this NASA Tech Briefs *issue, and the page number.*

Automated Detection of Streaks in Rocket-Engine Plumes

Transient events indicative of malfunctions are detected through processing of image data.

Marshall Space Flight Center, Alabama

A high-speed observer (HSO) system comprising a high-frame-rate digital video camera and a high-speed computer that processes the camera output has been developed for use in monitoring the exhaust plume of the space shuttle main engine (SSME) during tests. The HSO system is designed to analyze the digital video data to detect transient streaks and other anomalies in the appearance of the plume that are indicative of engine malfunctions. The basic HSO concept is also applicable to monitoring of transient phenomena in other settings.

In the original SSME application, combustion of hydrogen and oxygen yields nearly transparent plumes when the engine is functioning as intended. Bright streaks in the plumes, typically generated during combustion of contaminants in the hydrogen and/or oxygen, are potential indicators of abnormal events. Streaks can also be caused by combustion of debris generated by erosion of engine parts.

During an engine test, the computer in the HSO system processes the image data in real time to detect and differentiate anomalous plume events that occur during time intervals of the order of 5 ms. Such processing speed makes information on the state of the engine available nearly instantaneously; this information can be monitored by the test conductor and/or by a computer to determine whether the test should be terminated to prevent a catastrophic failure.

More specifically, image data are acquired, validated, saved, and analyzed to detect streaks, and the detected streaks are counted. The processed streak data are examined by expert-system software to determine whether the streaks violate criteria for acceptable engine operation during a sufficiently long time interval that they should be considered indicative of actual or potential trouble.

The hardware and software subsystems of the HSO system are easily reconfigurable, and off-the-shelf hardware and software can be used. The HSO system can be used for post-test analysis of all plume events as well as for monitoring during tests. Small, short-duration streaks can be evaluated against hardware inspection results and streaks correlated with hardware failures.

The HSO system can also be used to detect and analyze transient events (other than changes in image intensity) in settings other than testing of the SSME. Any event that can be recorded by an imaging device and recognized by software can be monitored. Examples include motions of objects, fluid leaks with visible manifestations, and fires.

This work was done by Tom Rieckhoff of **Marshall Space Flight Center** *and Michael O'Farrell and Mark Covan of United Space Alliance. Further information is contained in a TSP [see page 1].*

MFS-31500

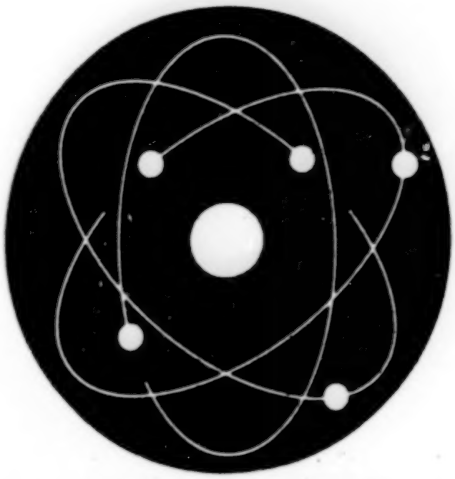

Physical Sciences

Hardware, Techniques, and Processes

Books and Reports

BLANK PAGE

Tiger Fibers for Enhanced Optical Sensing of Volatiles

Striped polymer coats on optical fibers would induce gratings upon exposure to analytes.

NASA's Jet Propulsion Laboratory, Pasadena, California

Improved fiber-optic transducers, denoted tiger fibers, have been proposed for sensing volatile compounds. Tiger fibers are so named because, as described below, their sensitive portions would be coated with periodically alternating stripes of different polymers, reminiscent of a tiger's stripes.

A related proposal is that of optical noses, reported in "Fiber-Optic Transducers for Distributed Sensing of Volatiles: An Optical Nose" (NPO-21105), *NASA Tech Briefs*, Vol. 25, No. 6 (June 2001), page 33. To recapitulate: An optical nose comprises mainly a fiber-optic transducer coupled to a hand-held optical time-domain reflectometer (OTDR). The fiber-optic transducer is an optical fiber coated with a polymer at one or more desired sensing locations along the fiber length. This polymer swells upon exposure to the volatile compound(s) that one seeks to detect [hereafter denoted "analyte(s)"]. The swelling induces a local mechanical strain in the fiber and, consequently, a local variation in the indices of refraction of the fiber core and cladding materials. The OTDR launches picosecond laser pulses into the optical fiber at one end. The index-of-refraction variations induced by the analyte(s) of interest at the sensing locations cause part of the incident laser light to be reflected. The OTDR makes time-resolved measurements of the intensity of the reflected laser light. For a given reflected pulse, the location of the corresponding sensing location is inferred from the measured round-trip pulse travel time. The drawback of optical noses is that the degree of swelling may be insufficient to afford acceptably high chemical sensitivity.

The tiger-fiber concept is also related to that of long-period fiber gratings (LPFGs), which have been used as temperature and chemical transducers. The core of a typical prior LPFG is fabricated with a photoinduced permanent periodic longitudinal variation of its index of refraction. Depending on the spatial period (of the order of tens to hundreds of microns, depending on the application), the fiber attenuates light of one or more known wavelengths more strongly than at other wavelengths.

A tiger fiber would incorporate features of both an optical nose and an LPFG. A tiger fiber would function similarly to a prior LPFG, but its core would not be fabricated with a permanent variation of its index of refraction. Instead, the fiber would be coated with stripes of a polymer that swells when exposed to the analyte(s), alternating with stripes of a polymer that does not swell when so exposed (see figure). The spatial pitch of the stripes would be made equal to the desired grating period. In the absence of the analyte, the fiber would transmit light with little attenuation. Exposure to an analyte would engender longitudinally periodic swelling that would induce corresponding periodic mechanical strains and periodic variations in indices of refraction of the fiber core and cladding materials, thereby causing the fiber to become an LPFG. The degree of the attenuation of light at the at the LPFG wavelength(s) would be related to the concentration of the analyte.

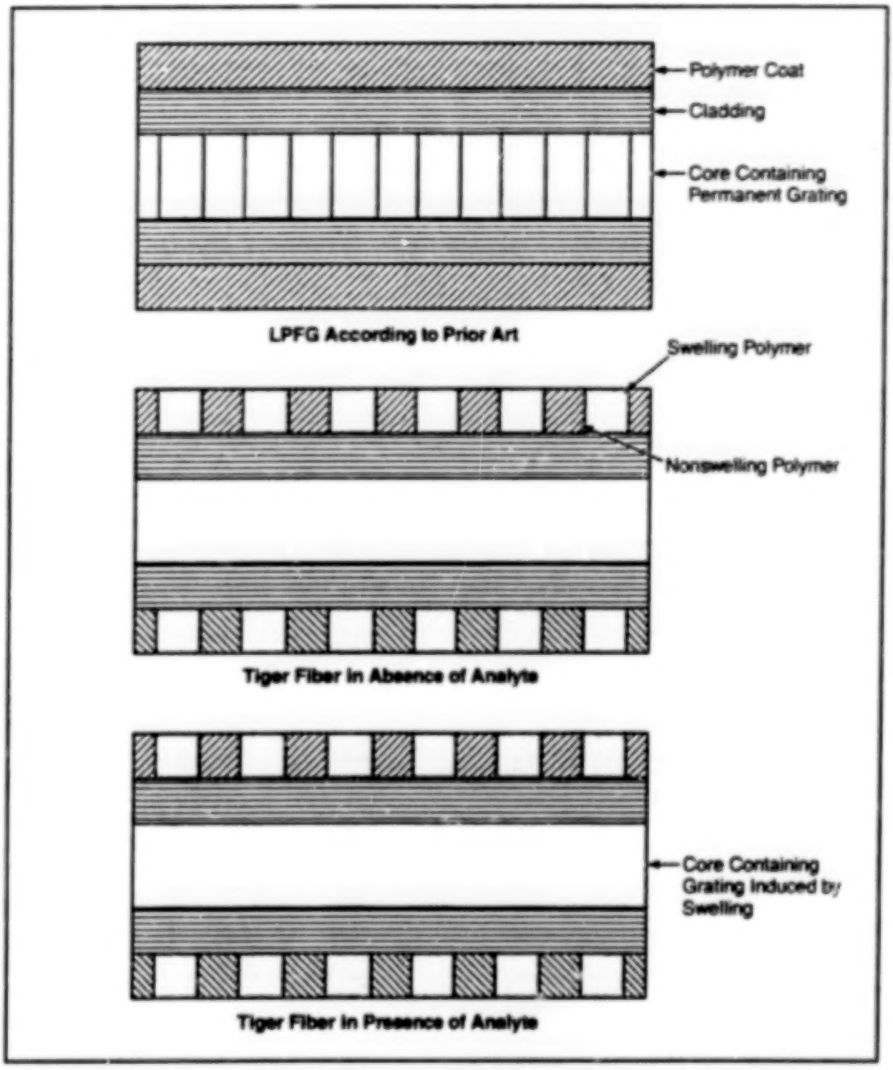

A Tiger Fiber would be coated with alternating stripes of a swelling and a non-swelling polymer. Swelling of one of the polymers on exposure to an analyte would induce a periodic longitudinal variation in the indices of refraction of the fiber core and cladding.

This work was done by Adrian Ponce and Dmitri Kossakovski of Caltech for **NASA's Jet Propulsion Laboratory**. *Further information is contained in a TSP [see page 1].*

NPO-21226

Thermocouple Rakes for Measuring Boundary-Layer Flows

Flows can be measured extremely close to surfaces.

John H. Glenn Research Center, Cleveland, Ohio

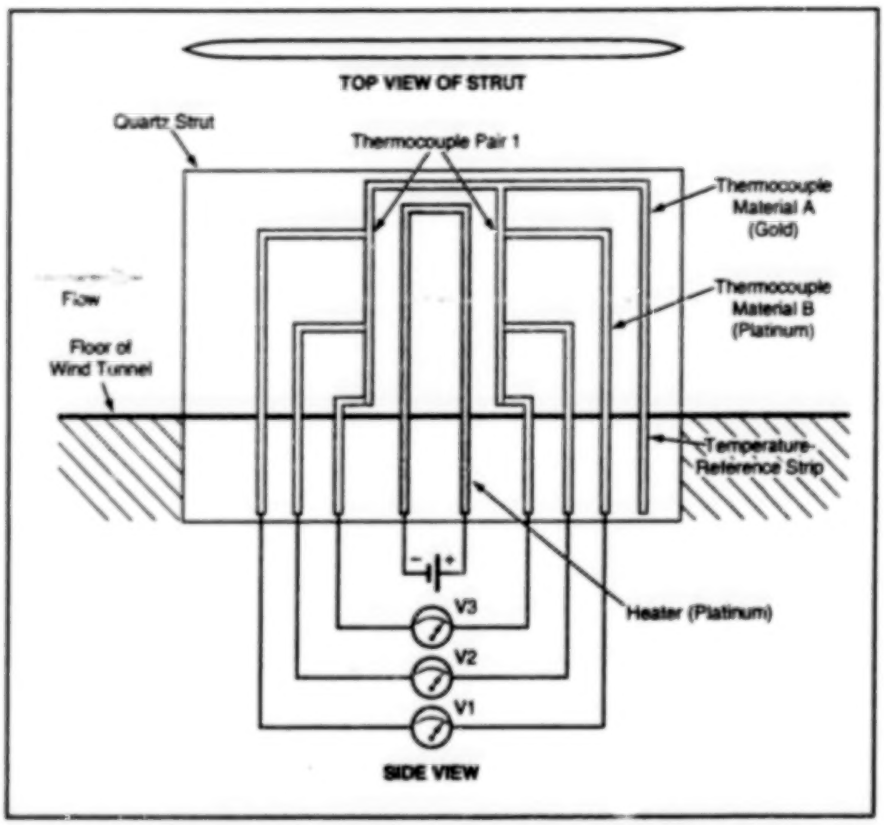

Figure 1. A Thin-Film Device Comprising a Heater and Thermocouples is affixed to a thin strut that is in the form of a constant-thickness airfoil with its span perpendicular and its chord parallel to the free-stream flow.

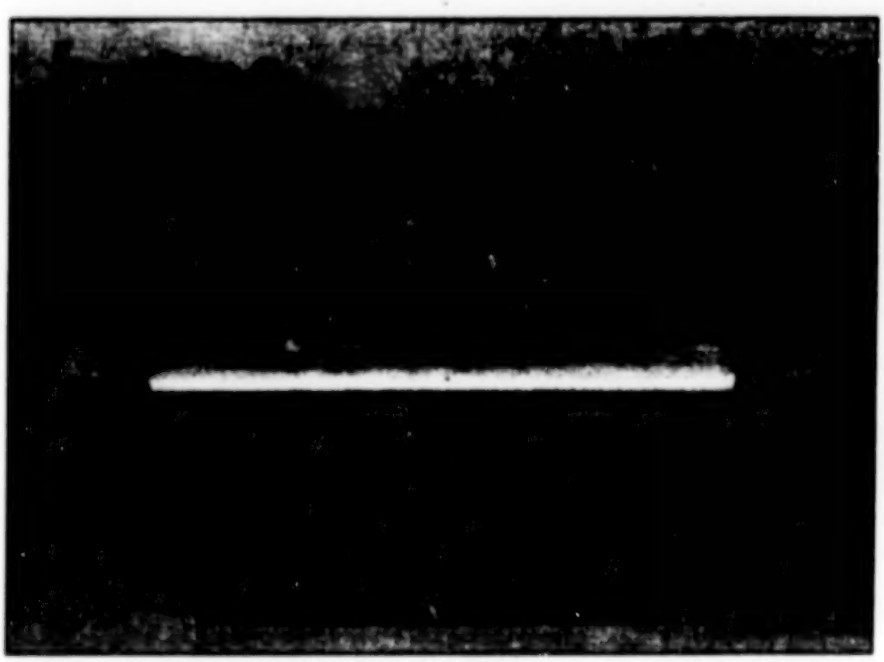

Figure 2. A Flow Sensor Is Mounted on an Adaptor that can be bolted into the floor of a wind-tunnel test section in an arrangement similar that of Figure 1. The lead wires of the thermocouple pairs are connected to the pins of a standard 50-pin ribbon cable connector by use of silver-filled epoxy.

Thin-film devices that comprise heaters in combination with thermocouples have been developed for measuring flow velocities extremely close to solid surfaces, at several distances from the surface of interest. Devices that perform this function are denoted generally as "boundary-layer rakes." The measurement data acquired by boundary-layer rakes are needed for calculating viscous shear forces, for developing mathematical models of turbulence to be used in computational fluid dynamics, and as feedback in some flow-control systems.

The present devices overcome the deficiencies of devices used heretofore for the same purpose. Those devices (which include rakes of total-pressure-probes and of hot-film and hot-wire anemometers) are incapable of measuring flow quantities closer than about 0.02 in. (≈0.5 mm) from solid surfaces. In contrast, the present devices can be miniaturized to enable them to measure as close as 0.0002 in. (≈0.005 mm) from surfaces — a hundredfold improvement. Also, in comparison with the prior boundary-layer rakes, these devices are sturdier.

Figure 1 schematically depicts a device of this type as mounted for a typical wind-tunnel experiment. In this example, the heater is made of platinum and the thermocouples are made of platinum/gold pairs; however, other heater and thermocouple alloys could be used. The heater and thermocouples are mounted on a side surface of a strut made of quartz or other low-thermal-conductivity material. Equal numbers of thermocouples are placed both upstream and downstream of the heater so that the voltage generated by each pair at the same distance from the surface is indicative of the difference in temperature between the upstream and downstream thermocouple locations.

In the absence of flow, the upstream and downstream thermocouples are at the same temperature, so that the voltages generated by the pairs (V_1, V_2, and V_3 in this example) are zero.

In the presence of flow, the temperature of each upstream thermocouple exceeds that of the downstream thermocouple in the same pair because the downstream thermocouples are warmed by air that has passed over the heater. Hence, in the presence of flow, the voltages are nonzero; in general, they are

approximately proportional to the flow velocity. Moreover, if the flow reverses, the polarity of the output voltages also reverses. Consequently, unlike hot-film and hot-wire anemometers, a device of this type indicates reversal of flow.

The number of thermocouple pairs can be as many as needed, up to a practical limit set by the number of alloy traces that can be patterned on the quartz surface. Also the miniaturization of a device of this type is limited by the capability for fine-line photolithography. Figure 2 depicts a working prototype. These devices could be batch-fabricated on quartz or other low-thermal-conductivity substrates at relatively low cost. These devices could be particularly useful for measuring flows on the surfaces of airplanes, in ventilation ducts, in jet aircraft engines (most importantly, for detecting incipient compressor stall), and in automotive engines.

This work was done by Danny P. Hwang, Herbert A. Will, and Gustave C. Fralick of **Glenn Research Center**. *Further information is contained in a TSP [see page 1].*

Inquiries concerning rights for the commercial use of this invention should be addressed to NASA Glenn Research Center, Commercial Technology Office, Attn: Steve Fedor, Mail Stop 4–8, 21000 Brookpark Road, Cleveland, Ohio 44135. Refer to LEW-16999.

Seed-Wing Flyers for Exploration

Scientific instruments would be dispersed from aloft by use of miniature autogyros.

NASA's Jet Propulsion Laboratory, Pasadena, California

Small instrumented, free-flying (unpowered) rotary aircraft have been proposed for use in gathering scientific data from hazardous or inaccessible terrain on remote planets as well as on Earth. These aircraft are called "seed-wing flyers" because they would resemble winged seeds (e.g., maple seeds) in both appearance and aerodynamic behavior.

The class of seed-wing flyers would constitute a subset of biomorphic explorers — mobile exploratory robots, inspired by natural biological forms, that would be equipped with microsensors and associated electronic circuits (including communication circuits). Biomorphic explorers and related concepts have been described in several previous articles in *NASA Tech Briefs*, the most relevant being "Biomorphic Explorers" (NPO-20142), Vol. 22, No. 9, (September 1998), page 71; "Earthworm-like Exploratory Robots" (NPO-20266), Vol. 22, No. 6, (June 1998), page 11b; "Insectile and Vermiform Exploratory Robots" (NPO-20381), Vol. 23, No. 11, (November 1999), page 61; and "Biomorphic Gliders" (NPO-20677), Vol. 25, No. 4 (April 2001), page 65. Seed-wing flyers could be dropped in large numbers over the terrain of interest from aircraft, spacecraft, or perhaps other biomorphic flyers. The dropped seed-wing flyers would then descend, spread out, and land at numerous locations on the terrain.

The flight of a winged seed is characterized by autorotation: The aerodynamic forces on the wing cause the wing and the rest of the seed to rotate in such a way as to generate lift, which retards descent. A winged seed or an artificial object shaped like a winged seed is as effective in retarding descent as is a parachute with a radius equal to the wing span. The underlying aerodynamic principle is essentially the same as that of helicopters and autogyros.

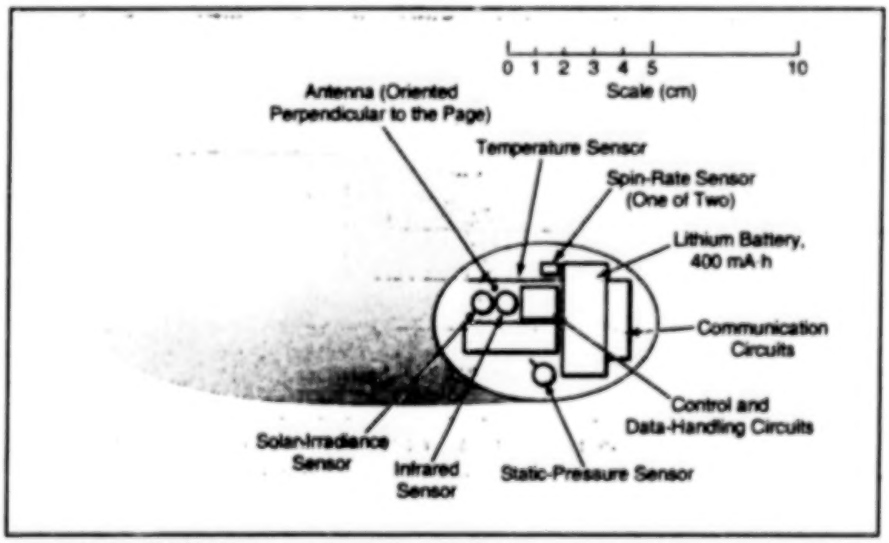

A **Typical Seed-Wing Flyer** would contain scientific instruments and electronic circuitry. The scale in this view is based on sizes of some devices that are now commercially available and other devices that are expected to become available in the near future.

Seed-wing flyers would be perhaps the simplest of all artificial flight systems in that like natural winged seeds, they would contain no moving parts, no control systems, and very few structural elements. In the intended application, seed-wing flyers would be used as alternatives to instrument packages dropped with parachutes. As in the case of parachutes, payload mass fractions could be large — greater than 80 percent in some cases. Seed-wing flyers would afford some advantages over parachute-dropped instrument packages, including the following:

- Unlike a parachute-dropped instrument package, a seed-wing flyer would have an unobstructed overhead view; in a situation in which there was a need to measure solar irradiance, such a view would be essential.
- A seed-wing flyer could be built from relatively few parts.
- A seed-wing flyer could be deployed reliably by simply dropping it; in contrast, deployment of a parachute entails a substantial deployment mechanism.
- At least on a small scale, a seed-wing flyer would likely be less massive than would be a parachute-dropped instrument package of similar functionality.

This work was done by Santa Thakoor of Caltech and Carlos Miralles of AeroVironment for **NASA's Jet Propulsion Laboratory**. *Further information is contained in a TSP [see page 1].*

NPO-20676

Boundary Conditions for Computing Flows of Real Gas Mixtures

It is possible to suppress errors that arise in a simplistic formulation.

NASA's Jet Propulsion Laboratory, Pasadena, California

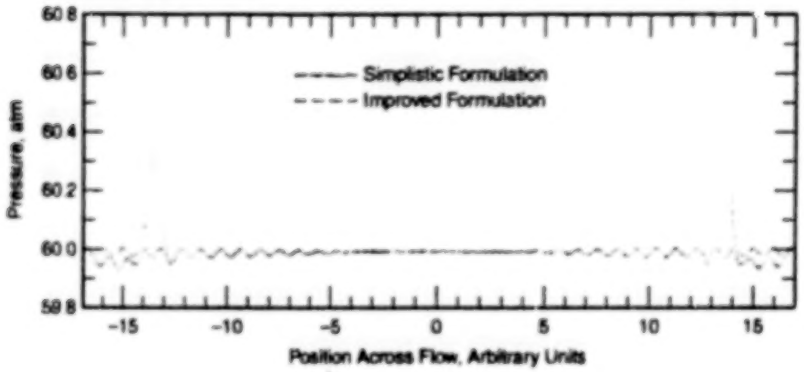

Pressure as a Function of Position Across the Flow was computed after an acoustic wave reached the nonreflecting side boundaries. The simplistic formulation yielded spurious reflected waves. The small, high-spatial-frequency oscillations are artifacts of a numerical-integration procedure used to solve the equations of flow.

An improved formulation of equations of flow of a general gas mixture includes consistent boundary conditions that are applicable to real gases. An analysis of prior formulations, with focus on boundary conditions, led to the conclusion that boundary conditions based on ideal mixtures and/or perfect gases can lead to errors in computed flows of real gases. The improved formulation makes it possible to achieve greater accuracy in computation of flows of real (including chemically reactive) gas mixtures, and is expected to be especially beneficial in computing flows of supercritical fluids like those in diesel engines, gas turbine engines, rocket engines, supercritical-fluid extraction processes, and crude oil under high pressure.

The improved formulation is derived from equations of conservation of mass, chemical species, energy, and momentum of a real gas mixture. These equations have the typical form of the Navier-Stokes equations augmented by the species- and energy-conservation equations and by an equation of state, except that the species and energy equations contain additional terms: The traditional Fick mass-diffusion and Fourier heat-diffusion terms are now respectively complemented by the Soret and Dufour terms that represent, respectively, the thermal contribution to diffusion of species and the transport of heat due to gradients in concentrations of species.

The conservation equations are for general viscous fluids; however, the boundary conditions are calculated from equations of inviscid flow (Euler equations) augmented by species and energy equations. Characteristic boundary conditions are derived from a wave decomposition of the Euler equations, and wave-amplitude variations are determined from the prescribed boundary conditions on the flow variables in conjunction with a general equation of state for a real gas.

The improved formulation was tested in computations of the one-dimensional propagation of acoustic waves in a flowing supercritical mixture of nitrogen and heptane in a two-dimensional domain with nonreflecting boundaries. The results obtained with this formulation were compared with those from another formulation in which real-gas thermodynamic properties were simplistically substituted into characteristic equations derived previously for a perfect gas. The waves computed in the improved formulation were found to leave the computational domain with minimal reflection at a subsonic outflow boundary, whereas the waves computed in the simplistic formulation exhibited significant reflections at the boundaries (see figure).

Although the superiority of the improved formulation has been shown by this test, caution is in order because the characteristic-wave analysis inherently incorporates the assumption that elliptic terms act only as corrections to an essentially hyperbolic operator. Thus, diffusional terms are not parts of the consistent-boundary-condition analysis, but are used in the governing equations once a solution is sought. The condition of weak ellipticity may not always be satisfied when thermal-diffusion effects are large enough to augment the effective thermal conductivity to the point of making heat diffusion processes comparable in magnitude to convective processes.

This work was done by Josette Bellan, Nora Okong'o, and Kenneth Harstad of Caltech for **NASA's Jet Propulsion Laboratory**. *Further information is contained in a TSP [see page 1].*

NPO-20970

Direct Methanol Fuel Cells With Aerosol Feed

Relative to liquid feed, aerosol feed would result in less methanol crossover.

NASA's Jet Propulsion Laboratory, Pasadena, California

Direct methanol fuel cells that would function with aerosol feed (instead of all-gas or all-liquid feed) have been proposed. As explained below, aerosol feed would afford the advantages of liquid feed, while reducing or eliminating some of the disadvantageous effects of liquid feed.

The invention of liquid-fed, polymer-electrolyte-membrane (PEM), direct methanol fuel cells (DMFCs) was something of a technological breakthrough; the performances of such fuel cells greatly exceed those of gas-fed methanol fuel cells because (1) the concentrations of methanol in the feed liquids (aqueous solutions of methanol) are much greater than those in the feed gases and (2) the increased concentrations result in increased transfers of mass to anodes.

In a liquid-feed PEM DMFC, methanol is supplied in excess to a catalytic anode on one side of a membrane/electrode

assembly. Desirably, all or most of the methanol should diffuse into the anode and partially react. Undesirably, some of methanol diffuses through the polymer-electrolyte membrane from the anode to the cathode — a phenomenon called "methanol crossover." This phenomenon reduces cathode performance and fuel efficiency. It also becomes necessary to use a dilute methanol feed solution to minimize crossover. The depletion of methanol from the already dilute solution adjacent to the catalytic anode surface further reduces performance by increasing the resistance to transfer of mass into the cathode. The use of a dilute methanol solution also tends to result in flooding of the cathode with water; this flooding further reduces performance and leads to loss of water through evaporation.

Aerosol feed was conceived with the major objectives of reducing methanol crossover, increasing the concentration of fuel at the anode, and minimizing accumulation of water at the cathode. "Aerosol" as used here denotes a suspension of droplets of nearly pure methanol in a suitable gas, which could be the CO_2 generated at the anode during normal operation. With a suitably controlled aerosol feed, very little methanol would be available at the membrane electrode for crossover, yet the concentration of the little methanol present at the catalytic anode surface would be high, as needed for high performance.

The sizes of the methanol droplets in an aerosol feed would lie between 0.1 and 10 μm. The aerosol feed for a given fuel cell could either be generated by one or more atomizers or equivalent devices located within the fuel cell near the anode, or else generated outside the fuel cell and blown in to the anode. Generating the aerosol outside the fuel cell would be advantageous in that the sizes of the methanol droplets could be controlled to optimize performance.

Control of droplet sizes would be important for the following reasons: During flow to the catalytic anode surface, some droplets of methanol would undesirably coalesce through the combined effects of diversion of the flow by some fuel-cell components, inertial deviation of droplets from deviated flow trajectories, and Brownian motion of the smallest droplets. To preserve the benefits of aerosol feed, it would be preferable to prevent the pores of the catalyst and the backing paper of the anode from becoming saturated with methanol, because if saturation were to occur, the anode would behave as in a liquid-feed cell, and crossover would rise substantially as a result. Minimization of droplet coalescence can prevent saturation. The quantitative measure of the tendency toward coalescence and saturation is called "collection efficiency," and it depends on droplet size and flow speed, as depicted in the upper part of the figure. One could minimize the collection efficiency by use of a droplet-size conditioner in the form of a porous diffuser, electrostatic separator, packed bed, or other device that would filter large droplets out of the flow, as indicated schematically in the lower part of the figure.

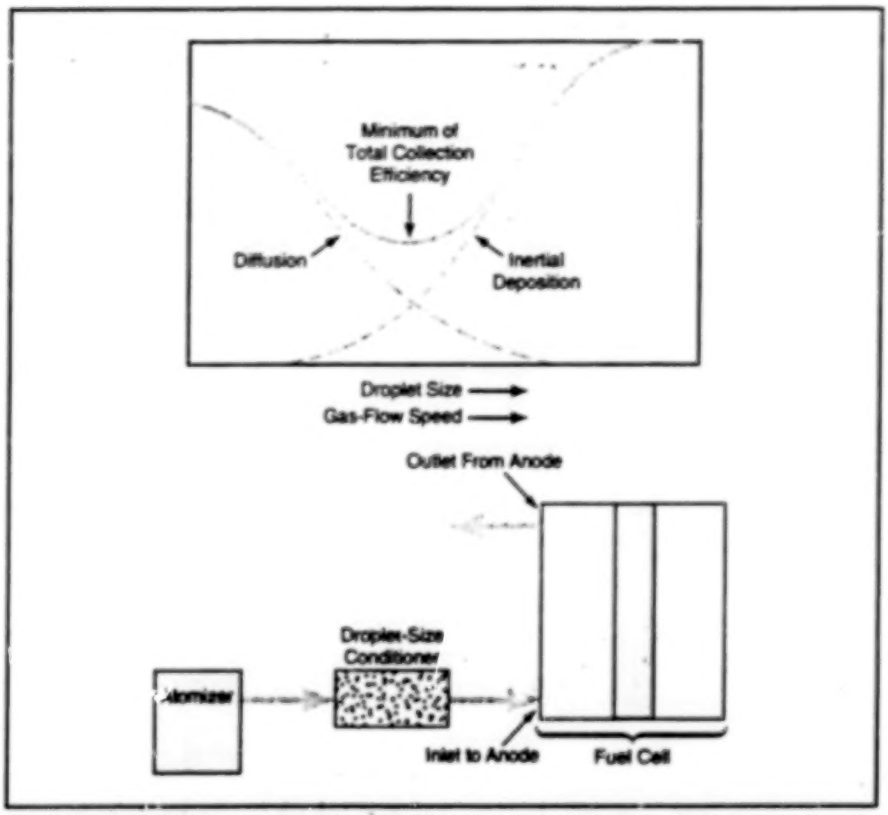

The Collection Efficiency is affected by diffusion and inertial deposition, which depend primarily on droplet size and flow speed, respectively. By filtering out the largest droplets, a droplet-size conditioner would reduce the collection efficiency and thus the tendency toward saturation of the anode.

It would be necessary to vent some of the aerosol flow to limit the buildup of pressure caused by the generation of CO_2. To limit the loss of methanol from such venting, the vent flow would be sent through a filter, membrane, or packed bed, which would cause methanol droplets to coalesce and would collect the coalesced droplets for recycling. However, unlike in a liquid-fed DMFC, there would be no need for a relatively bulky and heavy gas/liquid separator to separate the CO_2 from the methanol in the flow downstream of the cathode; consequently, it should be possible to make an aerosol-fed fuel-cell system smaller and less massive than a liquid-fed system of comparable performance.

This work was done by Andrew Kindler, Sekharipuram Narayanan, and Thomas Valdez of Caltech for **NASA's Jet Propulsion Laboratory**. *Further information is contained in a TSP [see page 1].*

In accordance with Public Law 96-517, the contractor has elected to retain title to this invention. Inquiries concerning rights for its commercial use should be addressed to

Technology Reporting Office
JPL
Mail Stop 249-103
4800 Oak Grove Drive
Pasadena, CA 91109
(818) 354-2240

Refer to NPO-20745, volume and number of this NASA Tech Briefs *issue, and the page number.*

Long-Life Stratospheric Balloon System With Altitude Control

There would be no venting of helium or dropping of ballast.

NASA's Jet Propulsion Laboratory, Pasadena, California

A proposed improved balloon system for carrying scientific instruments in the stratosphere would include a lightweight, ambient-pressure helium balloon and a vented infrared Montgolfiere (see figure). [An infrared Montgolfiere is an ambient-pressure warm-air balloon, named after the familiar fire-heated hot-air balloons invented by the Montgolfier brothers. An infrared Montgolfiere is heated primarily by the Sun during the day, and/or by infrared radiation from relatively warm surface of the Earth at night.] The system would feature controllability of altitude for taking scientific data, landing, or taking advantage of favorable winds for relocation. The system would be designed for long life, but would weigh less (and therefore cost less) than do previously developed long-life balloon systems.

The advantages of the proposed system are best understood in the context of two prior classes of long-life, high-altitude balloons. One prior class is that of helium superpressure balloons, in which pressures above ambient are maintained in order to maintain constant densities and thus constant altitudes. The other prior class is that of infrared Montgolfieres (used by themselves, rather than in combination with ambient-pressure helium balloons according to the present proposal). Superpressure balloons must be strong, and thus heavy, to maintain their interior pressures above ambient. Montgolfieres are not as efficient as helium balloons are and hence must be very large, and correspondingly heavy. A Montgolfiere by itself floats higher during the day than during the night, and thus is not well suited for observations for which altitude control is required. Altitude control for helium balloons has been effected by partial venting of helium (for descent) or dropping of ballast (for ascent), but these releases entail a tradeoff between controllability and longevity.

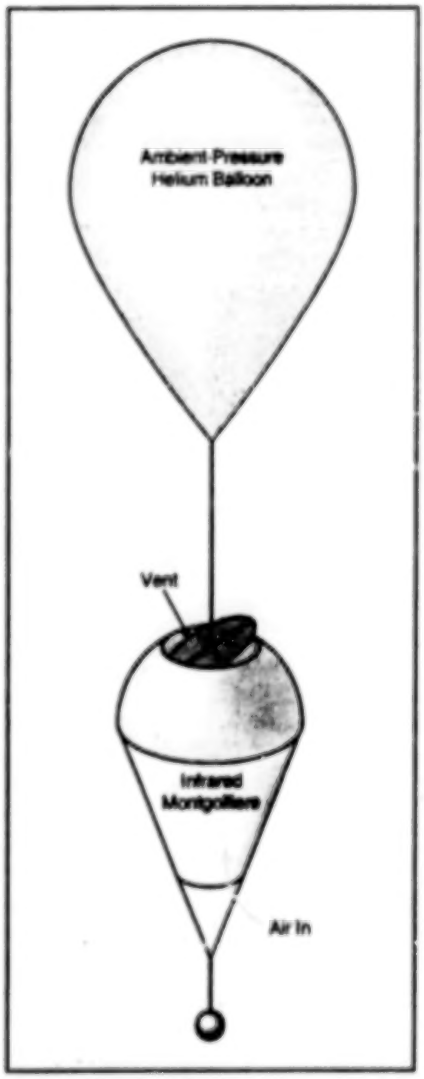

Two Different Balloons would be used together to take advantage of the differences between their diurnal variations in buoyancy.

In the proposed system, there would be no deliberate venting of helium or release of ballast. The ambient-pressure helium balloon would provide most of the lift during the day. The infrared Montgolfiere could be used to make up for the small decrease in buoyancy caused by nighttime cooling of the helium balloon, or to increase altitude. A vent in the top of the infrared Montgolfiere could be used to vary the buoyancy.

Masses and sizes of a conventional superpressure helium balloon and of the balloons in the proposed system have been calculated for a payload mass of 500 kg at the altitude where the ambient pressure is 0.01 bar (1 kPa). The total mass of the proposed system was found to lie between one-fifth and one-third of that of the superpressure helium balloon, the exact value depending on specific design parameters. Because the construction of an ambient-pressure balloon is much easier than is that of a superpressure balloon, the cost of the proposed system should be even lower than that indicated by the ratio of masses.

This work was done by Jack Jones of Caltech for **NASA's Jet Propulsion Laboratory**. *Further information is contained in a TSP [see page 1].*
NPO-20742

A Multifunctional Active-Excitation Spectral Analyzer

A portable, near-room-temperature instrument would optically probe chemical compositions of surfaces.

NASA's Jet Propulsion Laboratory, Pasadena, California

A highly sensitive, low-power, low-noise multifunctional active-excitation spectral analyzer (MAESA) that would span the wavelength range of 0.5 to 2.5 μm and would operate near room temperature is undergoing development. The fully developed MAESA is expected to be a portable and highly miniaturized version of a prototype of the instrument that has been demonstrated in a laboratory. The MAESA is intended primarily for use in remote sensing of chemical compositions of mineral surfaces on planets or on Earth.

The MAESA (see figure) would include a laser and associated optics for generating a beam of monochromatic light to illuminate a point or a line on a target. Other optics in the MAESA would image the target onto a rectangular focal-plane array (FPA) of InGaAs photodetectors, whereon a pixel or a column of pixels, would correspond to the illuminated target point or the illuminated target line, respectively. At the target, the illumination would excite Raman scattering, the spectrum of which would depend on (and which could be analyzed to estimate) the chemical composition of the target. The light returning from the target would be long-wavelength-pass filtered to remove the laser wavelength component, then focused onto a convex diffraction grating, which would spectrally disperse the remaining Raman-

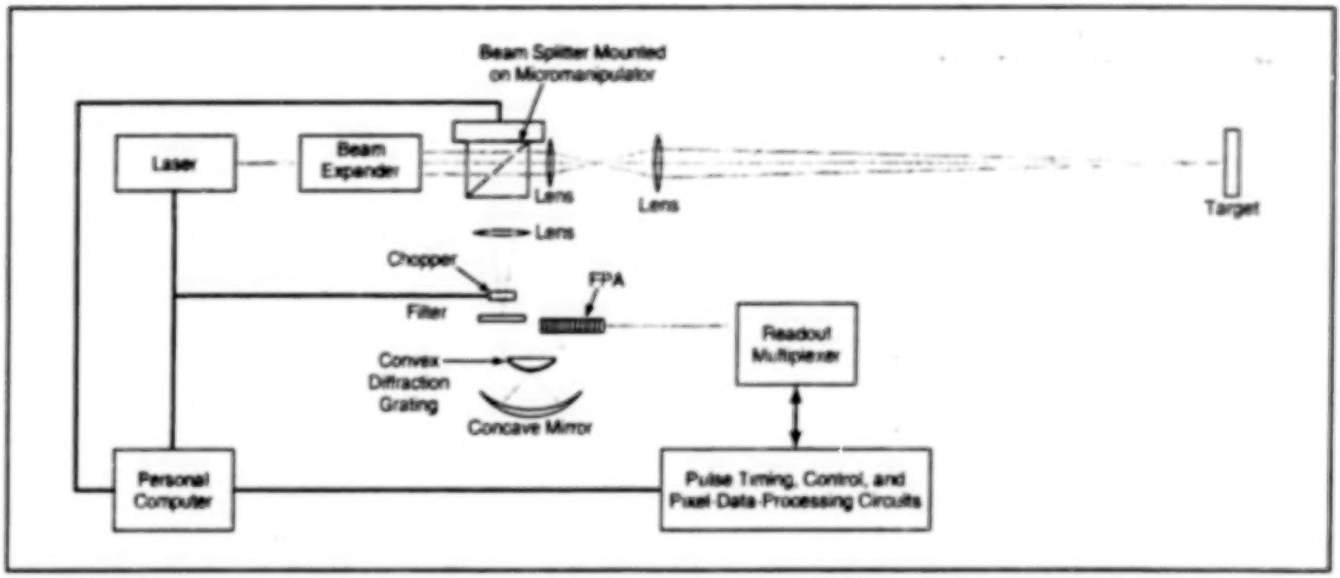

This **Block Diagram** depicts a simplified combination of features of the laboratory prototype MAESA and the contemplated fully developed version of the MAESA to illustrate the principle of operation.

scattered light along a row of the FPA. The InGaAs FPA (which could be a commercially available unit) would be hybridized with a custom-made silicon complementary metal oxide/semiconductor (CMOS) readout multiplexer integrated circuit. The output of the readout multiplexer would be sent to pixel-data-processing circuits.

The wavelength of the spectral component impinging on each pixel would be a known function of the position of the pixel along the row. Hence, by processing the readouts from all the pixels in this row at the same time, one could obtain a characteristic spectrum for estimating the chemical composition of the illuminated point on the target. Optionally, the readout multiplexer and the downstream data-processing circuitry could be made to repeat the readout and processing in a temporal sequence corresponding to successive rows of pixels, thereby building up spectrally resolved information about the chemical compositions of the target at all the target pixel locations along the column axis. A further option would be to deactivate the laser and replace the convex diffraction grating with a conventional curved mirror, in which case the MAESA would function as a conventional camera recording images in ambient visible and/or infrared light.

The advantage of using an FPA made of InGaAs (in contradistinction to photodetector arrays made of other semiconductors) are that InGaAs offers the potential for superior detectivity (D^*), without need for cooling, over the wavelength range of 0.5 to 2.5 μm, which range is not spanned by any other single active detector material. The high D^* enables high spectral (or alternatively, temporal) resolution and makes possible the wide dynamic range needed for detection of weak visible and infrared Raman spectra characteristic of materials of interest.

The convex diffraction grating would consist, more precisely, of three concentric subgratings. Each subgrating would provide spectral dispersion free of distortion in one of three wavelength subbands: 0.5 to 1.0, 0.8 to 1.6, and 1.25 to 2.5 μm, respectively. The grating would be fabricated in a micromachining process based on electron-beam lithography.

This work was done by Quisup Kim of Caltech for **NASA's Jet Propulsion Laboratory**. *Further information is contained in a TSP [see page 1].*
NPO-21143

Hand-Held Optoelectronic Particulate Monitors

Data on concentrations and sizes are obtained from diffraction of light.

Lyndon B. Johnson Space Center, Houston, Texas

Optoelectronic instruments are being developed for use in measuring the concentrations and sizes of microscopic particles suspended in air. The instruments could be used, for example, to detect smoke, explosive dust in grain elevators, or toxic dusts in industrial buildings. Like some older, laboratory-bench-style particulate monitors, these instruments are based on diffraction of light by particles. However, these instruments are much smaller; exploiting recent advances in optics, electronics, and packaging, they are miniaturized into compact, hand-held units.

The prototype instrument includes a miniature optical train targeted on a gas sample that contains particles to be detected. A light-emitting diode or laser diode generates a beam of light that is collimated by a first lens and passed through the gas sample. Forward-diffracted light produced by interaction of the beam with particles in the sample is collected by a second lens, which focuses the light onto one central circular and three concentric annular arrays of optical fibers. The fibers in each array carry the focused diffracted light to one of four photodiodes, so that the outputs of the photodiodes provide a coarse-resolution representation of the radial dependence of the diffraction pattern.

An aperture stop is placed in front of the second lens to attenuate the bright undiffracted beam. This aperture stop is an engineered low-reflectance, high absorbance, optical element in the form of a thin-film absorber less than 0.2 μm thick. It transmits only about 0.2 percent of the power of the undiffracted beam through to the second lens, while reflecting only about 0.1 percent and absorbing the rest. In so doing, it (1) reduces flare light that might otherwise cor-

rupt the dim diffraction pattern, (2) minimizes the undesirably strong spurious scattering of light that would occur if the undiffracted beam were allowed to be reflected back toward the sample at a substantial fraction of its original power, (3) minimizes spurious diffraction from stationary dirt particles, which eventually will come to adhere to the second lens, and (4) provides a low-power proportional sample of the undiffracted beam for use as an intensity reference, as explained next.

The central array of optical fibers carries light from the attenuated undiffracted beam to one of the photodetectors. The output of each of the other photodetectors is divided by the output of this photodetector, so that the diffracted-light reading from each annulus is converted to a ratio that is independent of the intensity of illumination. This ratiometric readout technique normalizes out the effects of fouling of surfaces and of fluctuations in the source of light. Furthermore, each ratio is directly proportional to the density of particles in the sample gas.

The three ratios and a reading proportional to the intensity of the undiffracted beam are displayed on a liquid-crystal readout device. In principle, the sizes of the particles can be estimated from the diffraction pattern; that is, from the ratios. The prototype does not contain the microprocessor that will be needed in a complete, fully designed unit to control the acquisition of data and compute the sizes of particles. The algorithm needed to compute the sizes has not yet been fully developed either, though it is known that the algorithm will likely call for diffraction ratios at more than three annuli.

The wavelength of illumination in the prototype is 670 nm. This limits quantitative measurements to particles larger than about 1 μm. A shorter wavelength would, of course, enable the measurement of proportionally smaller particles.

This work was done by Eric W. Saaski of Research International, Inc., for **Johnson Space Center**. *Further information is contained in a TSP [see page 1].*
MSC-22466

Using Laser Diodes to Characterize Force and Pressure Sensors

A proposed method of characterizing microphones and other pressure and force sensors would exploit the temporally varying forces of impingement of amplitude-modulated light beams from inexpensive laser diodes. What makes the method likely to be practical is the surprising fact that these forces, albeit small, are nevertheless large enough to enable quantification of the noise floors, sensitivities, and frequency responses of many modern pressure sensors. The time-averaged force of impingement of a pulsed beam of light on a surface is given by $F = SDP/c$, where S ranges from 1 for a totally absorptive (black) to 2 for a perfectly reflective surface, D is the pulse duty cycle, P is the peak power of the beam, and c is the speed of light. Hence, if one knows S, D, and P, it may be possible to determine the absolute sensitivity of the sensor. Even if one does not know one or more of these parameters, it should be possible to determine the relative sensitivities of different sensors by measuring their responses to the same modulated beam, or to determine the relative frequency response of a given sensor by measuring its output while sweeping the modulation frequency.

This work was done by Robert C. Youngquist of **Kennedy Space Center**. *Further information is contained in a TSP [see page 1].*

This invention is owned by NASA, and a patent application has been filed. Inquiries concerning nonexclusive or exclusive license for its commercial development should be addressed to the Technology Programs and Commercialization Office, Kennedy Space Center, (321) 867-4879. Refer to KSC-12183.

Books and Reports

DNS of a Supercritical H_2/O_2 Mixing Layer

This report discusses direct numerical simulations (DNS) of a mixing layer between supercritical flows of oxygen and hydrogen. The governing conservation equations were those of fluctuation-dissipation (FD) theory, in which low-pressure typical transport properties (viscosity, diffusivity and thermal conductivity), are complemented, at high pressure, by a thermal-diffusion factor. The Peng-Robinson equation of state was coupled to the conservation equations to obtain a closed system. The temperature/pressure regime was one in which both Kolmogorov and Batchelor scales could be resolved for pseudospecies (species with transport properties modified to enable the attainment of large enough Reynolds numbers). Notable among the simulation results was lack of transition to turbulence, attributed to two causes. First, a relatively large spanwise perturbation induces early small-scale formation, which destroys the coherence of the vortices formed through pairing and impedes entrainment and the further formation of small scales. The ultimate vortex resulting from the second pairing is weakened during this process. Second, the regions of large density-gradient magnitude formed both through the distortion of the initial density stratification boundary and through mixing of the two species act similar to material boundaries and damp small turbulent eddies. A comprehensive analysis of the results is presented as well.

This work was done by Josette Bellan, Kenneth Harstad, and Nora Okong'o of Caltech for **NASA's Jet Propulsion Laboratory**. *To obtain a copy of the report, "Direct Numerical Simulations of LOX/H_2 Temporal Mixing Layers Under Supercritical Conditions," see TSP's [page 1].*
NPO-30179

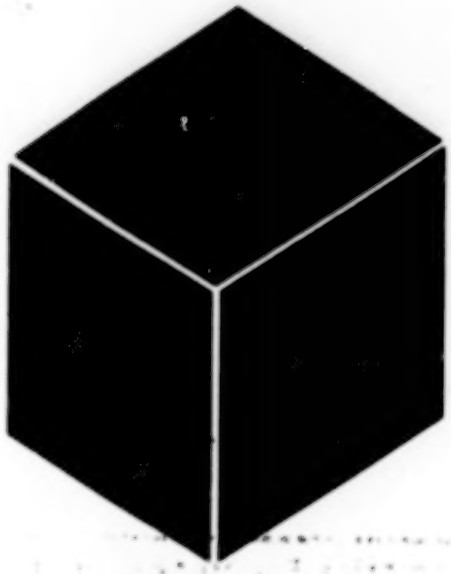

Materials

Hardware, Techniques, and Processes

28

BLANK PAGE

Annealing for Tailoring Au/GaN Schottky-Barrier Height

It should be possible to make metal/semiconductor contacts more reproducible.

NASA's Jet Propulsion Laboratory, Pasadena, California

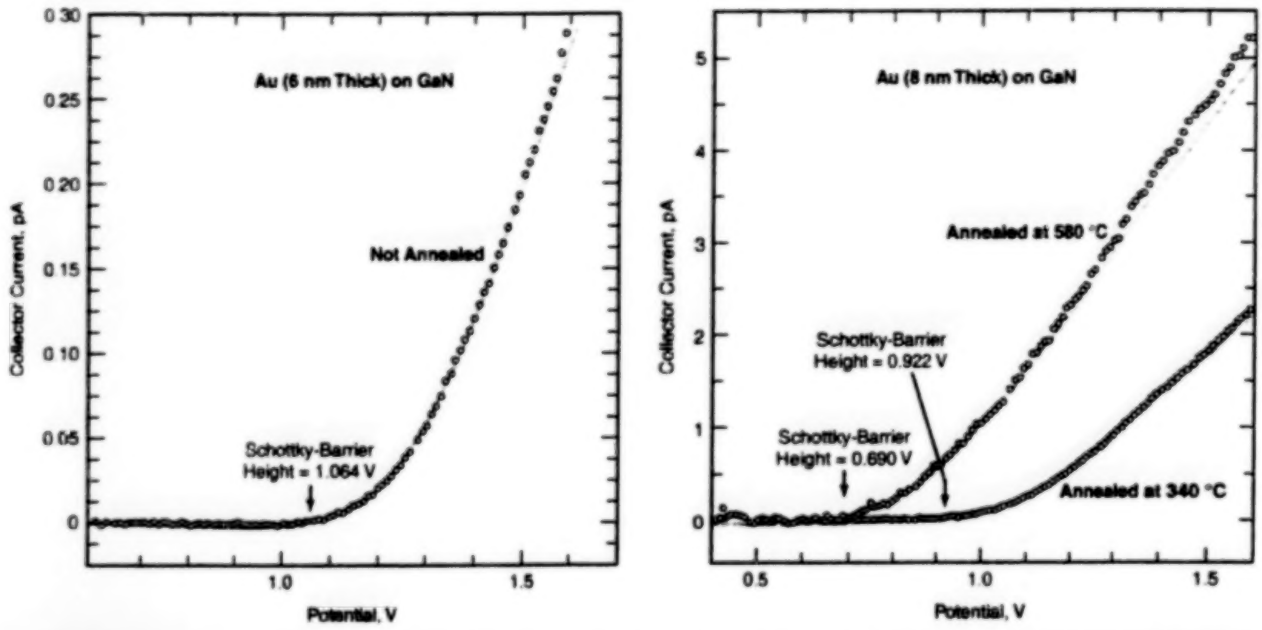

These BEEM Spectra of unannealed and annealed specimens show the effects of annealing on Schottky-barrier height and interface transmission.

Annealing has been found to be an effective means of tailoring the height of a Schottky barrier between gold and gallium nitride. This finding offers promise for the development of improved metal contacts on GaN semiconductors. Heretofore, the commercialization of GaN semiconductor devices has been impeded by difficulties of fabrication and by nonreproducibility of the Schottky-barrier heights and other properties of the metal/GaN interfaces. Now it appears that annealing may be the key to making GaN devices with smaller unit-to-unit variations of contact properties and, in particular, tailorability of Schottky-barrier heights over a wide energy range.

Prior attempts to tailor Schottky contact properties had focused on details of surface cleaning and of growth and bulk properties of GaN. These attempts were not successful: unit-to-unit variations were still observed, even after cleaning and growth under controlled conditions. Although the causes of these variations are still not fully understood, more recent studies led to a partial explanation and to the annealing approach: It appears that the growth of GaN can result in a near-surface region wherein there are nonequilibrium concentrations of vacancies in Ga and N sites. These concentrations depend on aspects of the growth process that are difficult to control. These vacant sites act, variously, as electron acceptors or donors within the GaN semiconductor. As such, these sites affect the Schottky contact properties.

It was hypothesized that annealing of GaN prior to deposition of metal could be beneficial for tailoring Schottky contact properties because by suitable choice of annealing conditions (time, temperature, and either nitrogen atmosphere or high vacuum), it should be possible to produce a surface region with (1) a desired composition somewhere within a range from Ga-rich to N-rich and (2) corresponding values of near-surface doping and Schottky-barrier height. This hypothesis was investigated in experiments on GaN specimens that were cleaned with HCl, then annealed prior to deposition of Au by vacuum evaporation. The specimens were then probed by ballistic-electron-emission microscopy (BEEM) for measurement of interface transmission efficiencies and Schottky-barrier heights. For comparison, some specimens were subjected to cleaning by HCl but not annealed. Other specimens were cleaned by other chemical treatments; these specimens were also not annealed. In the absence of annealing, neither the HCl treatment nor the other chemical treatments yielded substantial increases in interface transmission.

The figure shows a typical BEEM spectrum for a specimen that was not annealed, and for two other specimens that were annealed in ultrahigh vacuum for 15 minutes — one at a temperature of 340 °C and one at a temperature of 580 °C. Features of BEEM spectra can be correlated with interface properties. The voltage threshold for the onset of measurable current yields the interface Schottky-barrier height, and the magnitude of the current above this threshold indicates the fraction of the electrons injected by BEEM can cross the interface. This in turn gives information on the ideality of the interface, i.e., interface quality. Changes in these interface properties result in changes in features of the BEEM spectra. The figure shows that Schottky-barrier heights decreases, and interface transmission increases, as annealing temperature is increased. Other spectra taken after annealing at other temperatures confirm this trend. It has also been determined from BEEM spectroscopy that the starting interface properties and the direction of their change with temperature depend partly on the previous thermal history of the specimen. The changes in Schottky-barrier heights have been interpreted in terms of the creation of vacancies or the diffusion of vacancies toward the GaN surface.

This work was done by L. Douglas Bell and R. Peter Smith of Caltech for **NASA's Jet Propulsion Laboratory**. *Further information is contained in a TSP [see page 1].*
NPO-21008

Ceramics Made From Wood

Properties can be tailored in many different ways.

John H. Glenn Research Center, Cleveland, Ohio

The term "ecoceramics" (a contraction of "environment-conscious ceramics") denotes a class of ceramics made partly from wood-based products, which can include natural wood, sawdust, cardboard, and/or paper. In addition to the environmental advantage of renewability of the carbonaceous ingredients, the concept of ecoceramics offers an advantage of tailorability of the properties of the ceramic end products.

In the case of natural wood, the natural open cellular structures can serve as templates. Wood preforms can be laminated to optimize the toughnesses and strengths of the resulting ceramics. Alternatively or in addition, wood and sawdust layers can be alternated to obtain desired properties.

The wood-based preform of an ecoceramic object is pyrolized at a temperature of as much as 1,000 °C in a chemically inert atmosphere (nitrogen or argon). If the intended product is a silicon carbide-based ceramic, then the pyrolyzed preform is infiltrated with molten silicon or a molten silicon alloy. The temperature and time of infiltration depend on the type of preform and the composition of the infiltrating material: Typical infiltration temperatures are 40 to 50 °C higher than the melting temperatures of the infiltrating materials, and typical infiltration times range from 15 minutes to an hour. For example, infiltration by silicon at 1,450 °C for 30 minutes is sufficient for making ecoceramics from preforms derived from natural oak.

To make a porous silicon carbide-based ceramic, one can begin by dipping a preform derived from natural wood in an aqueous slurry that contains 40 to 60 percent of silicon or a silicon alloy powder, the balance comprising organic binders and water. After dipping in the slurry, the preform is dried, then heated in a furnace to a temperature above the melting temperature of the silicon or the silicon alloy. The silicon or silicon alloy melts and reacts with cell walls of the wood, yielding a porous structure.

It is also possible to make nonceramic carbon-matrix composite materials through infiltration of thermoplastic or thermoset resins into preforms derived from wood. In other variations on the basic theme, preforms derived from wood can be infiltrated with such diverse materials as organometallic polymers; oxide precursors (sols and slurries); molten binary, ternary, and higher oxides; metals; intermetallic compounds; ferro silicon; and combinations of the aforementioned materials. The infiltrants can be selected to provide hard and soft phases with desired thermomechanical, magnetic, electronic, piezoelectric, and/or wear properties. In yet another variation, small and simply shaped ecoceramic parts can be joined to make larger, more complexly shaped, and/or functionally graded parts.

This work was done by Mrityunjay Singh of Dynacs Engineering Co., Inc., for **Glenn Research Center**. *Further information is contained in a TSP [see page 1].*

Inquiries concerning rights for the commercial use of this invention should be addressed to NASA Glenn Research Center, Commercial Technology Office, Attn: Steve Fedor, Mail Stop 4–8, 21000 Brookpark Road, Cleveland, Ohio 44135. Refer to LEW-17043.

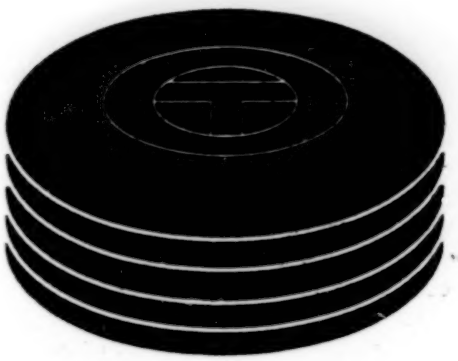

Computer Programs

Mechanics

Mathematics and Information Sciences

BLANK PAGE

Mechanics

Program Computes Pointing Corrections for a Radiotelescope

TLC is a computer program that determines corrections for radiotelescope-pointing errors associated with tilts and elastic deformations. These errors occur because for rotation in azimuth, a radiotelescope is mounted on wheels that move on a circular track that deviates from perfect flatness. TLC processes radiotelescope field data through smoothing, filtering, segment-fitting, trend-removal, Fourier-transform, and high-pass-filtering algorithms to generate a lookup table that contains the pointing corrections. The field data in question are readouts from four inclinometers, the relative positions of the inclinometers, and readouts from an azimuth-angle encoder. Written in the Matlab software system, TLC is a user-friendly program that provides a graphical user interface that enables even an unfamiliar user to proceed, step by step, to the final result.

This work was done by Wodek Gawronski and Erin Maneri of Caltech for **NASA's Jet Propulsion Laboratory**. *Further information is contained in a TSP [see page 1].*

This software is available for commercial licensing. Please contact Don Hart of the California Institute of Technology at (818) 393-3425. Refer to NPO-21135.

Mathematics and Information Sciences

Software for Analyzing Root Causes of Process Anomalies

Root Cause Analysis (RoCA) is a computer program that assists analysts in understanding the root causes of process anomalies. As used here, "process anomalies" includes incidents that have caused, or that can potentially cause, injuries to personnel, damage to facilities, abnormal costs, or delays in processing. RoCA could be used, for example, in industry to investigate anomalies in production and by government agencies and airlines in investigating airplane accidents. Older software developed to aid such investigations offers limited capabilities for mapping the contribution of each root cause to a given process anomaly. Unlike the prior software, RoCA not only identifies root causes of process anomalies but also supports the identification of trends over multiple anomalies.

RoCA implements a causal-network format for root-cause analysis. The analyst can specify a causal structure (that is, what root causes contributed to each ultimate effect). The analyst can also specify the strengths of relationships between causes and effects. Given the causal structure and qualitative strength-of-relationship judgements, Bayesian networks can be used to evaluate the relative contributions of various root causes to a given anomaly. RoCA makes it possible to perform causal analysis to be performed on individual events and for the results of analyses of multiple events to be summarized and analyzed to support trend analysis.

RoCA also maintains an event database and provides for the entry of new events into the database as well as for editing the names, locations, times, or other attributes of previously entered events. An analyst can display and edit an analysis on a time line of a sequence of events; thus, the analyst can concentrate on the flow and causes of events rather than on background details or on the details of computer-code representations of causes. RoCA also enables communication of information about events among analysts.

In a RoCA analysis, an analyst breaks down an investigation of a complicated event into investigations of smaller event components. Each event component represents a relevant factor that constitutes a piece of the puzzle in the event investigation and that the analyst considers useful to include in the analysis. By creating smaller units that describe aspects of the event and by specifying the causal relationships among them, the analyst can structure the analysis in such a way that anyone reviewing it can understand it. In a RoCA analysis, the network and time-line displays force the analyst to be explicit about any assumptions concerning what caused what and what happened when. Two or more analysts sharing their respective network and time-line displays can see and comprehend each other's assumptions.

RoCA can produce reports of many different types that can help in the identification of trends. Using these reports, an analyst can view data in a variety of ways and identify potential trends in the data that may warrant further investigation for systemic root causes. The analyst can enter a potential trend into the RoCA database and associate the trend with a set of events.

RoCA is written in Microsoft Visual Basic, using the Microsoft Jet/Access database drivers. RoCA utilizes interface-control software from FarPoint, DataDynamics, KL Group, and AddSoft.

This program was developed by Tim S. Barth and Lisa Grace Kestel of **Kennedy Space Center**; *Robert Fung and Brendan Del Favero of Prevision, Inc.; and Donna M. Blankmann-Alexander and Jeffrey R. Ewald of United Space Alliance. Further information is contained in a TSP [see page 1].*

In accordance with Public Law 96-517, the contractor has elected to retain title to this invention. Inquiries concerning rights for its commercial use should be addressed to

Robert Fung
Prevision, Inc.
120 N. Redwood Drive
San Rafael, CA 94903

Refer to KSC-12142, volume and number of this NASA Tech Briefs *issue, and the page number.*

Ex — Software for Numerical Computation in Native Oberon

"Ex" is the name of a library of software modules from which one can rapidly develop prototype or production versions of efficient numerical-computation application programs in the Native Oberon programming environment. Mathematical constructs that can be represented and processed by use of Ex modules include both integer and non-integer rational, real, and complex numbers; vectors; matrices; and the arithmetic, algebra, and calculus of the aforementioned quantities.

Native Oberon (which is so named for literary and historical reasons) is a fully functional operating system developed and maintained by the Institute for Computer Systems at ETH-Zürich, Switzerland. It runs on Intel-compatible personal computers and can be downloaded at no cost from the ETH Web site *http://www.oberon.ethz.ch/native/*. Native Oberon can also function as an X Window application program running under the Linux operating

system. The Oberon operating system is written in the Oberon language, which is a fully functional object-oriented descendant of the Pascal programming language. Oberon features the readability of Pascal and is designed to be "safe" in the sense that it minimizes errors early in the development of an application program.

The software modules in Ex are grouped into three tiers: a set of lower-level modules, an intermediate interface module, and a set of higher-level modules. The set of lower-level modules provides base types for numbers used in numerical analysis; specifically, integer, rational, real, and complex numbers are defined. The integers are defined as a subset of the rational numbers, which are defined as a subset of the real numbers, which, in turn, are defined as a subset of the complex numbers. Also defined are associated vector and matrix types, e.g., integer vectors and complex matrices. The arithmetic operators "+", "-", "*", "/", "DIV," and "MOD" and the assignment operator ":=" have all been overloaded (in the computer-programming sense), as appropriate, enabling the writing and facilitating the maintenance of clean code.

The intermediate interface module defines the base type for an Ex object. It also provides a means to make Ex objects, their extensions, and the Ex base types persistent.

The set of higher-level modules contains subsets of modules to implement various objects, functions, and operations, as follows.

- *Data structures* — queues, stacks, lists, and trees, which are Ex objects;
- *Mathematical functions* — numbers, series, calculator math, and matrix math; and
- *Calculus* — integrals, derivatives, ordinary differential equations, and optimization, for both the classical (i.e., integer) and fractional calculi.

Unlike the interfaces of the other tiers, which are expected to undergo little to no change with further development of Ex, the modules in this tier will likely grow and evolve as new functions and capabilities are added.

Software packages similar to Ex have been developed previously [e.g., Linear Algebra Package (LaPACK) in the FORTRAN language], but not in Oberon. Thus, Ex is expected to enhance the value of Oberon as an alternative to other languages for developing numerical-computation application programs.

This program was written by Alan D. Freed of **Glenn Research Center**. *Further information is contained in a TSP [see page 1].*

Inquiries concerning rights for the commercial use of this invention should be addressed to NASA Glenn Research Center, Commercial Technology Office, Attn: Steve Fedor, Mail Stop 4–8, 21000 Brookpark Road, Cleveland, Ohio 44135. Refer to LEW-17064.

Mechanics

Hardware, Techniques, and Processes

BLANK PAGE

Improved Piezoelectrically Actuated Microvalve

The improvements are intended to ensure less leakage and true normally-closed operation.

NASA's Jet Propulsion Laboratory, Pasadena, California

Efforts are underway to implement an improved design of the device described in "Normally Closed, Piezoelectrically Actuated Microvalve" (NPO-20782), *NASA Tech Briefs*, Vol. 25, No. 1 (January 2001), page 39. To recapitulate: This valve is being developed as a prototype of valves in microfluidic systems and other microelectromechanical systems (MEMS). The version of the valve reported in the cited previous article (see Figure 1) included a base (which contained a seat, an inlet, and an outlet), a diaphragm, and an actuator. With the exception of the actuator, the parts were micromachined from silicon. The actuator consisted of a stack of piezoelectric disks in a rigid housing. To make the diaphragm apply a large sealing force on the inlet and outlet, the piezoelectric stack was compressed into a slightly contracted condition during assembly of the valve. Application of a voltage across the stack caused the stack to contract into an even more compressed condition, lifting the diaphragm away from the seat, thereby creating a narrow channel between the inlet and outlet.

The improvements are being pursued because of the following deficiencies of the previous version of the valve:

- The valve-seat design was marginal in that dirt particles easily became stuck between the diaphragm and the tops of sealing rings, contributing to leakage.
- By virtue of the placement of the inlet orifice under the actuator, the inlet flow and pressure opposed the sealing force, thereby reducing the ability to seal against high pressure with low leakage.
- The piezoelectric actuator stack could not be machined as precisely as could the silicon parts. As a consequence, if the valve cap (the item designated the actuator housing in Figure 1) was flexible and the piezoelectric stack was thicker than the actuator housing, then the valve could not be actively opened. If the piezoelectric stack was thinner than the actuator housing, then the valve would always be open.

Figure 2 depicts some aspects of the improved version of the valve. The inlet is repositioned from the previous version, such that now the inlet flow and pressure contribute to sealing and thus to the desired normally-closed mode of operation. The piezoelectric actuator stack, and the cap have been redesigned to conform to this pressure-aided-sealing design. The valve seat has been redesigned to replace the former blunt-cross-section sealing rings with knife-edge sealing rings that would be less susceptible to trapping of particles between the rings and the diaphragm. The micromachined parts of the improved design are assembled by room-temperature indium hermetic bonding.

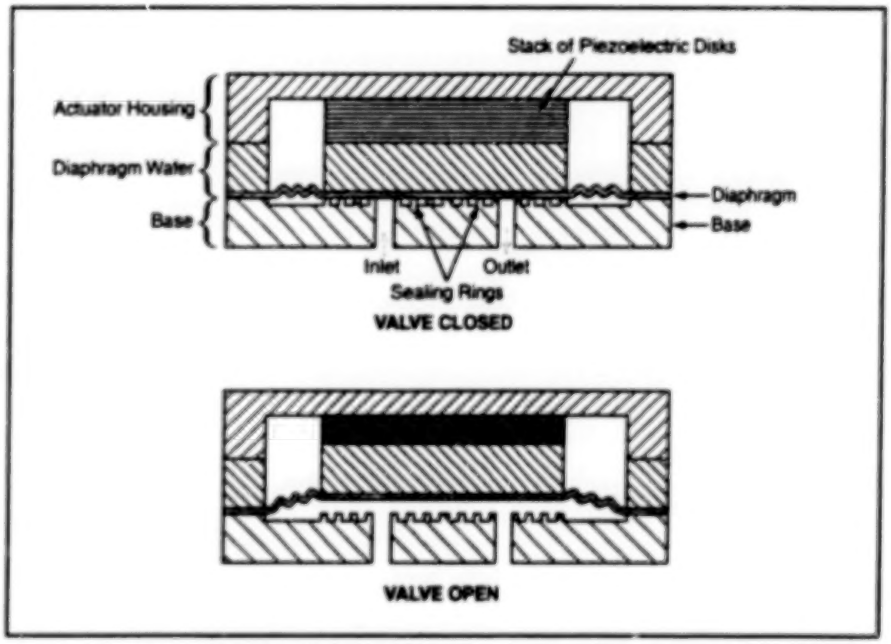

Figure 1. The Previous Version of the Valve, like the present version, was opened by applying a voltage that caused the piezoelectric actuator to contract slightly.

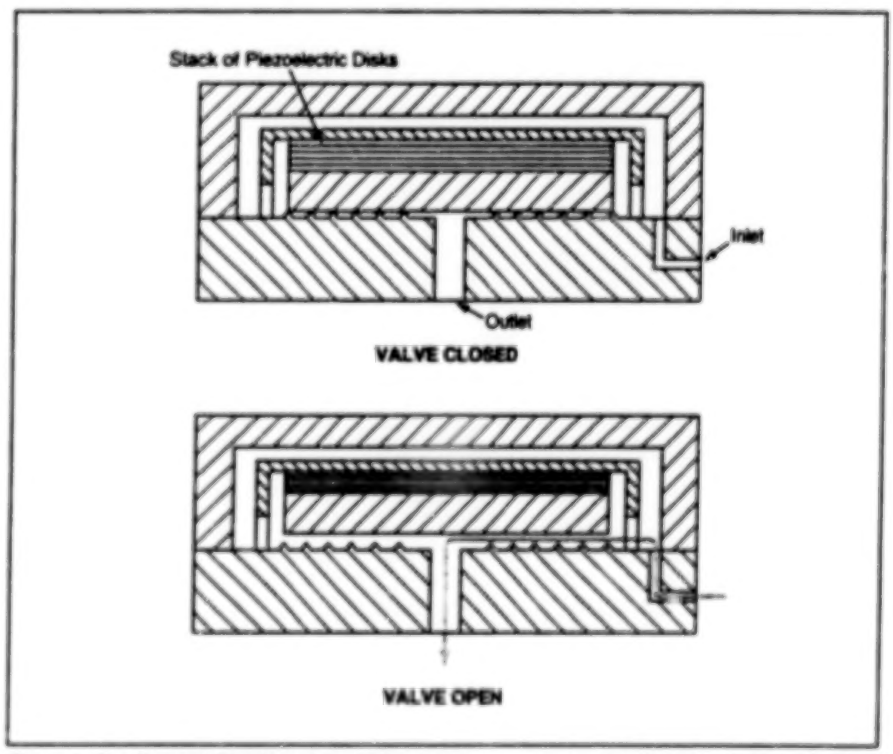

Figure 2. The Present Version of the Valve features a pressure-aided-sealing design and other improvements intended to overcome the deficiencies of the previous version.

This work was done by Eui-Hyeok Yang and David Blame of Caltech for **NASA's Jet Propulsion Laboratory**. *Further information is contained in a TSP [see page 1].*

NPO-30158

Instrumented Bolt Measures Bending Moments Within Itself

The direction as well as the magnitude of bending can be determined.

Marshall Space Flight Center, Alabama

The Ultrabend bolt is a specially designed bolt instrumented with strain gauges (see figure) that are connected into twin Wheatstone-bridge circuits. The geometric arrangement of the strain gauges is such that by suitable electrical switching of the Wheatstone-bridge circuits, these circuits can be made to either (1) suppress responses to bending and torsional stresses while putting out signals indicative of axial preload or (2) suppress responses to axial and torsional stresses while putting out signals indicative of the magnitude and direction of the bending moment in the bolt. Switching between these two measurement modes is accomplished by use of field-effect transistors controlled by a logic circuit.

The strain gauges are positioned and oriented orthogonally about the cylindrical axis of the bolt. In the bending-measurement mode, the root sum square of the outputs from the Wheatstone bridges is proportional to the magnitude of the bending moment in the bolt. At the same time, the arctangent of the ratio between the bridge outputs is the angle between the plane of bending and one of the radial coordinate axes defined by the positions of the strain gauges.

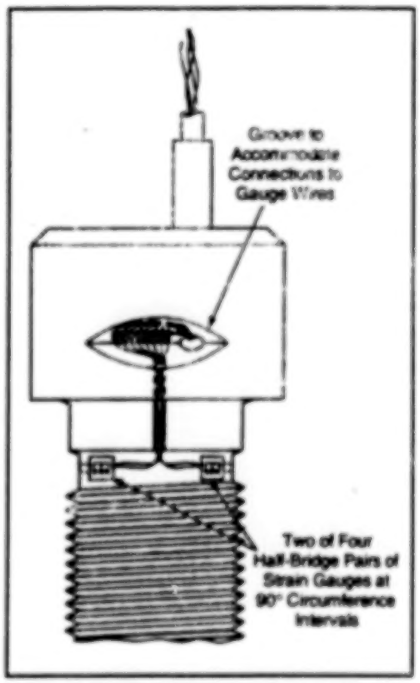

Pairs of Strain Gauges located at 90° intervals are connected into Wheatstone-bridge circuits so as to respond to either bending or axial preload in the bolt.

This work was done by Douglas E. Smith, Peter D. Totman, Randy L. Everton, Paul A. St. Jean, Marvin D. Bunderson, Mark R. Egget, and Randy Borgstrom of ATK Thiokol Propulsion, Inc., for **Marshall Space Flight Center**.

Title to this invention has been waived under the provisions of the National Aeronautics and Space Act [42 U.S.C. 2457(f)] to ATK Thiokol Propulsion, Inc. Inquiries concerning licenses for its commercial development should be addressed to

Thiokol Propulsion Patent Office
(435) 863-3511

Refer to MFS-31609, volume and number of this NASA Tech Briefs *issue, and the page number.*

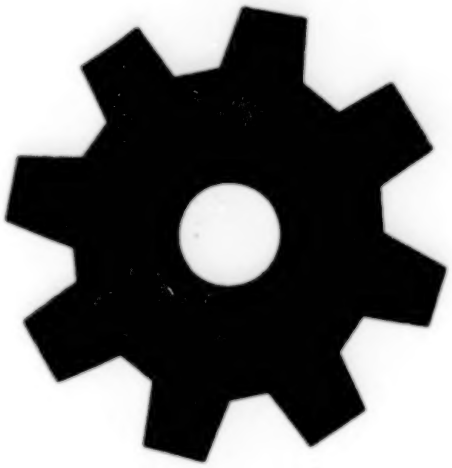

Machinery

Hardware, Techniques, and Processes

Books and Reports

Ice-Melting Probe Using Steam and Jets of Hot Water

This probe would overcome some of the deficiencies of prior ice-melting probes.

NASA's Jet Propulsion Laboratory, Pasadena, California

An improved probe has been proposed for burrowing vertically into ice for scientific exploration of polar icecaps, glaciers, and the like. The predecessor of the improved probe is a Philbert probe, which contains an electric heater to melt the ice in contact with it and thereby make it descend through the ice under its own weight. A Philbert probe also contains a mechanism from which the wires for the electric heater and any sensors in the probe are paid out behind the probe; these wires become sealed into the overlying ice as the probe descends. The two major drawbacks of a Philbert probe are that (1) it tends not to go straight down and (2) a plug of dust, sand, rock, and/or other debris tends to build up in the meltwater ahead of the probe, eventually becoming large enough to halt the descent by interrupting the heat-transfer interface between the vehicle nose and the ice. The improved probe is designed to eliminate these drawbacks.

Like a Philbert probe, the improved probe would include an electric heater and a mechanism for paying out wires connecting the probe to instrumentation on the surface. However, the manner of heating and the means of propulsion would differ greatly from those of a Philbert probe. Moreover, propulsion would involve cyclic (rather than continuous) operation. In comparison with a Philbert probe or other probe that depends on continuous melting, the improved probe would be more energy-efficient because less energy would be lost to the far field through gradual conduction; instead of melting the surrounding ice continuously at a slow rate, the improved probe would aggressively apply intense heat and melt only small portions of the ice for short intervals. In this manner, less heat would be lost to the far field.

The probe would contain a plug of ferrous metal that would be free to move vertically in a cavity within the probe. The plug would be heated by a resistive heating coil; this coil would also serve as an electromagnet coil that, when energized, would hold the plug at the top of the cavity. When the coil was de-energized, the hot plug would fall down in the cavity, which would be partly filled with water. Contact between the plug and the water would cause an explosion of super-saturated steam that would increase the pressure in the reservoir significantly, which in turn, would expel hot water/steam through orifices at the base of the reservoir leading to the nose.

These orifices would lie in a spherical nosepiece that would be free to spin, and the orifices would direct the flow of hot water/steam in the manner of turbine blades to make the nosepiece spin. The spin would ensure that the jets play over the entire frontal face of ice below the probe, melting the ice and stirring up any nonmelting debris so that the debris would become suspended in the liquid water and would be displaced by the probe as it moved down. The spherical nosepiece could be counterweighted, so that it would always cut downward in the absence of any nonmelting obstacle and would return the vehicle to downward movement immediately after passing an obstacle.

There would be another cavity rearward of (above) the water/steam cavity wherein the plug moves. This upper cavity would be kept filled with hydrogen and oxygen gases generated by electrolysis of water. Passages in the side wall of the probe would allow flow between this cavity and the front (lower) end of the probe. During the steam explosion, most of the hot water forced out of the water/steam cavity would rise along these passages, heating the side wall well above the melting temperature and pressurizing the gas in the upper cavity. This gas would act somewhat as a regulator that would maintain the probe at a modest overpressure relative to the ambient ice.

The electrolysis electrodes would be energized via the same wires as those for the heater/magnet. When the upper cavity was full of gas, the water level in the cavity would fall below the electrodes, stopping the electrolysis; thus, the volume of gas would, in effect, regulate itself. If the passages leading to the electrolysis chamber became clogged with debris, the debris could be cleared by sparking a hydrogen/oxygen explosion in the chamber.

The heating of the side wall would melt the ice in contact with the side wall, freeing the probe to fall into the cavity excavated below by the jets of hot water. Upon completion of expulsion of water from the water/steam cavity, the probe would have descended by an amount comparable to the dimension of the water/steam cavity. The next operating cycle would then begin.

This work was done by Brian Wilcox, Partha Shakkottai, and Wayne Zimmerman of Caltech for **NASA's Jet Propulsion Laboratory**. *Further information is contained in a TSP [see page 1].*

NPO-20894

Lightweight, Low-Backlash Robot Wrist With Epicyclic Drive

Several design features contribute synergistically to versatility and efficiency.

Lyndon B. Johnson Space Center, Houston, Texas

A unique lightweight wrist with three degrees of rotational freedom has been developed as a prototype of wrists for future anthropomorphic robots that would perform a variety of tasks on Earth and in outer space. The three degrees of freedom (two rolling, one bending) intersect at the center of the wrist. Included in the wrist is a power transmission with an epicyclic ring-gear configuration that enables efficient packaging and provides a wide internal passage through the center of rotation for routing of wires and drive cables. The power transmission combines low-backlash planetary gearing and a triple-input differential with a triple-load-path, cable-driven output stage that generates minimal radial bearing loads and no thrust (that is, axial) bearing loads.

The forearm portion of the wrist contains three high-performance motors — one for each input to the differential. The motors are mounted side by side, with their shafts parallel to the axis of the forearm and with room between them to route wires through the center of rotation. The motions in the three degrees of freedom are coupled; in other words, all three motors contribute to the output motion of each axis. As a result, the load capacity of the wrist for each degree of freedom can be as much as three times that of a wrist of traditional design in which each degree of freedom is actuated by a single dedicated motor. From a slightly different perspective, if one takes advantage of the possibility of combining the outputs of all three motors to

actuate a given degree of freedom, then one can use motors with a maximum power, size, and weight of only one-third of those that would otherwise be needed.

Each motor drives one of the input pinions of the ring-gear epicyclic transmission. Each input pinion is supported on both ends to reduce (in comparison with support on one end) shaft-flexing and bearing loads. Each input pinion drives two ring gears. For compactness, the ring gears are not supported by bearings; instead, each pair of ring gears is supported by its drive pinion and by two freely spinning (idler) pinions. The pinions bear all the radial loads on the ring gears. Pairs of ring gears are separated by low-friction washers to reduce wear.

Cables are wrapped around the ring gears and around mating pulleys. The ring gears in each pair are wrapped with a single cable and are loaded against a drive pinion in opposite directions to suppress backlash. Cables are terminated inside pulleys with preloading devices to compensate for thermal expansion and wear. Each cable is routed immediately around an adjoining pulley to change its direction without imposing thrust or radial load on any of the pulleys or gears, even under preload. Cables are wrapped immediately from one pulley to the next, minimizing the total length of cable and reducing susceptibility to stretch and thermal expansion. To minimize adverse effects of flexing and wear of cables, the diameters of the pulleys are made more than 30 times the diameter of the cables.

This work was done by Joseph Matteo of Matteo Automation and Robotics Co. for **Johnson Space Center**.

In accordance with Public Law 96-517, the contractor has elected to retain title to this invention. Inquiries concerning rights for its commercial use should be addressed to

Matteo Automation and Robotics Co.
721 Summit Lake Court
Knoxville, TN 37922
Tel. No. (423) 777-0577
Fax No. (423) 777-0578

Refer to MSC-23005, volume and number of this NASA Tech Briefs *issue, and the page number.*

Books and Reports

Pneumatic Accelerator for Launching a Spacecraft

A report proposes the development of a ground-based launch-assist apparatus that would accelerate a spacecraft to a speed of about 270 m/s. The apparatus would include a track along which the spacecraft would ride on a sled coupled to a large piston driven by compressed air along a tube (more precisely, a concrete tunnel lined with stainless-steel sheet) below the track. The connection between the sled and the piston would be made via a coupling plate that would slide along a slot on top of the tube. The slot would seal after passage of the coupling plate. As described thus far, the apparatus could be characterized as a modern, high-acceleration, high-speed version of pneumatic drives with slot connections to rail cars that were used in Europe during the 1840s. The apparatus would include commercially available compressors and valves, and the tube would be designed and built mostly according to familiar concrete and steel construction practices. The apparatus is intended to be a relatively inexpensive interim substitute for a magnetic-levitation launch-assist system that is expected to take considerably longer to develop and to be capable of accelerating spacecraft to greater speeds.

This work was done by Dale E. Lueck and Clyde F. Parrish of **Kennedy Space Center**. *To obtain a copy of the report, "Closed End Launch Tube," see TSP's [page 1].*
KSC-12237

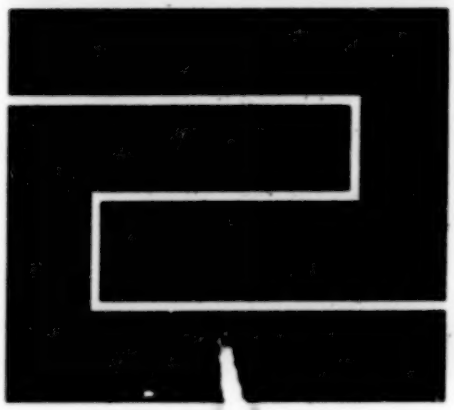

Fabrication Technology

Hardware, Techniques, and Processes

BLANK PAGE

Electrical Monitoring of Thicknesses of Semiconductor Wafers

Electrical fuses would be implanted at depths corresponding to desired thicknesses.

John H. Glenn Research Center, Cleveland, Ohio

A technique based on electrical-continuity measurements has been proposed as a means of monitoring and controlling the thicknesses of semiconductor wafers during lapping, polishing, and etching. The technique is expected to contribute to the development of microelectromechanical systems by making it possible to lap and polish wafers with precision greater than has been achieved previously, thereby further making it possible to fabricate wafers of unprecedented thinness (thicknesses of 5 μm or possibly even less). Unlike some prior techniques for measuring the thicknesses of semiconductor wafers, this technique does not entail the time-consuming intermittent stopping of processing to take measurements. Also, in comparison with most prior techniques, this technique offers the potential for greater precision at lower cost.

The technique involves preparing a wafer by forming one or more thin electrical conductor(s) within it at a depth that corresponds to the desired final thickness. During processing of the wafer, one would monitor the electrical resistance(s) of the conductor(s) to detect an increase in resistance as an indication that conductor material had been removed and thus the removal of material from the wafer had brought the wafer to the desired thickness. The increase in electrical resistance could serve as a control signal to stop the removal (lapping, polishing, or etching) process.

The figure depicts salient aspects of the technique in more detail at several stages of processing. There would be two wafers: the target wafer (the one to be thinned to a specified thickness) and a carrier wafer. By use of photolithography, one or more hole(s) of depth equal to the desired final thickness would be etched into the target wafer from its back side. Thin strips of metal (to serve as the electrical conductors) would be deposited and patterned on the back side; the strips would extend continuously from one edge of the wafer to the opposite edge and would extend all the way into the hole(s).

The thickness-controlling etched holes (dimples) are located in dead spaces on the target substrate. Such dead spaces are the grids that define the edge of individual chip cells. Therefore, the dimples do not reside within active areas of the chip or substrate.

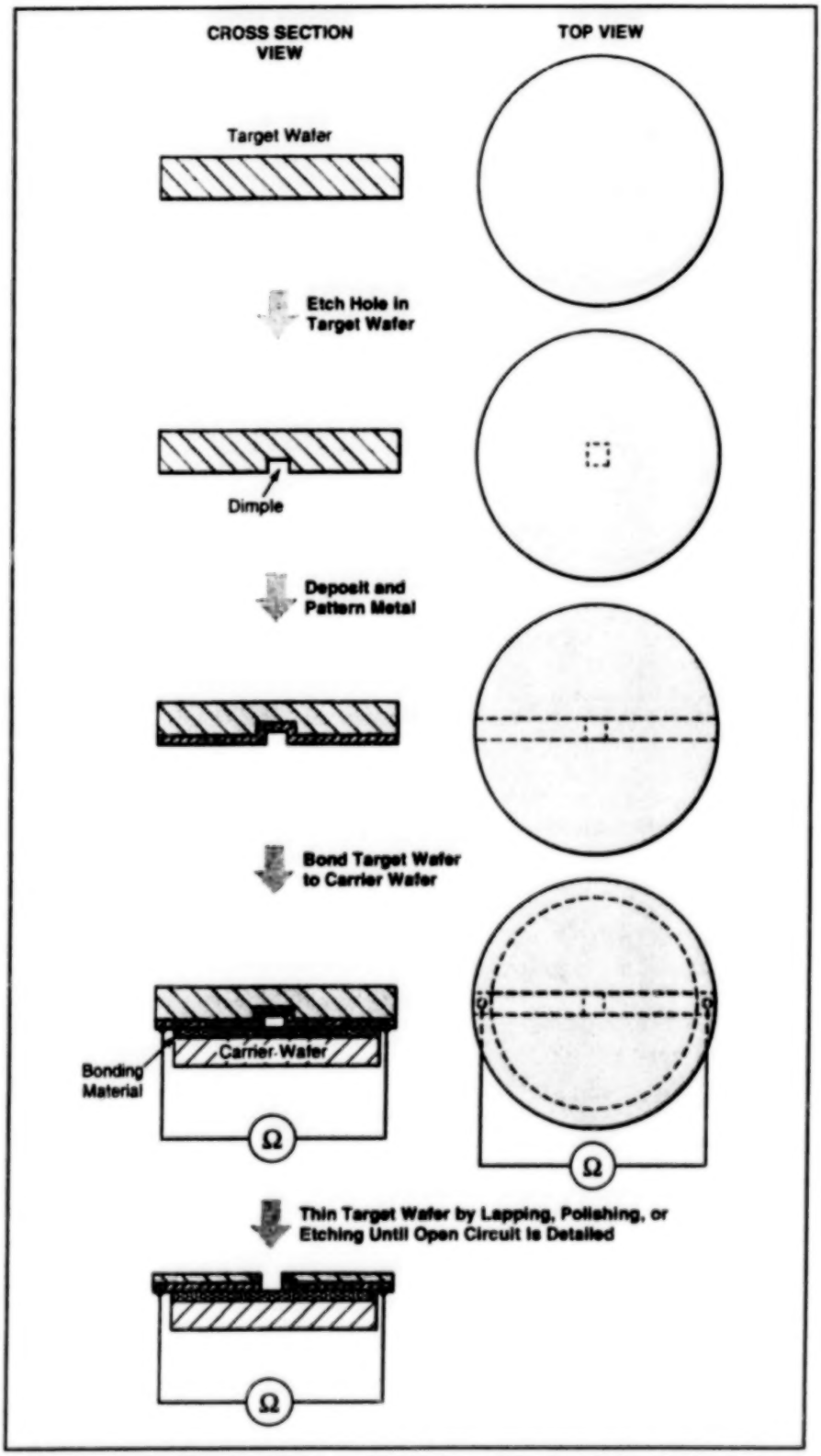

A Thin Conducting Strip deposited in an etched hole would be disrupted by thinning the target wafer to the thickness corresponding to the depth of the hole. The disruption of the strip would be detected via the concomitant increase in electrical resistance (possibly to the point of an open circuit) of the strip. [Note that the drawings are not to scale. The dimple is much smaller (few microns in diameter) than is depicted here.]

The carrier wafer would either be made of, or coated with, an electrically insulating material, and would have a diameter slightly less than that of the target wafer. The back side of the target wafer would be bonded to a face of the carrier wafer so that the carrier wafer could serve as a platform to hold the target wafer during processing to thin the target wafer. Because of the smaller diameter of the carrier wafer, the ends of the electrical conductor(s) on the target wafer would protrude slightly past the edge of the carrier wafer and would thus be accessible for measurement of electrical resistance. During processing, target-wafer material would be removed from the front side of the target wafer. Processing would be continued until the aforementioned increase in electrical resistance occurred.

This technique offers two fabrication options. It may be possible to selectively dissolve the carrier substrate and the conducting strips, thereby releasing the thin target wafer for further processing. Also, the carrier wafer and the conducting strips can become functional components of the final device.

This work was done by Robert S. Okojie of **Glenn Research Center**. *Further information is contained in a TSP [see page 1].*

Inquiries concerning rights for the commercial use of this invention should be addressed to NASA Glenn Research Center, Commercial Technology Office, Attn: Steve Fedor, Mail Stop 4–8, 21000 Brookpark Road, Cleveland, Ohio 44135. Refer to LEW-17022.

Two Techniques for Removing Core-Drill Debris

Both techniques contribute savings in time and money.

Lyndon B. Johnson Space Center, Houston, Texas

Two alternative techniques make it possible to remove core-drill debris more rapidly and efficiently than was previously possible. Either technique is a vast improvement over the prior art. For industries in which ultrasonic core drills are used, these two techniques are expected to result in savings of time and money.

Typically, an ultrasonic core drill includes a diamond-coated coring tool that vibrates vertically at a frequency of 20 kHz. The drill can be used dry or with a coolant. The drill generates debris that often becomes trapped in the coring tool. In the situation that prompted the development of the two present techniques, technicians were having difficulty cleaning a coring tool. In order to clean the tool, they had to stop the drill, remove the tool, and use a thin, stiff wire to push out the trapped debris or, if necessary, pick the pieces out by hand. The procedure was tedious. Inasmuch as it is necessary to recalibrate an ultrasonic drill each time it is disassembled and reassembled, the task of cleaning was all the more time-consuming.

The two present techniques make the task of cleaning the coring tool easier and faster. The first technique makes it possible to leave the drill in place during cleaning — a decided advantage in that the need for recalibration is eliminated. To utilize this technique, the tool must be modified first. Two slots are machined on opposite sides of the coring tool, creating a convenient outlet for trapped debris and providing technicians with an easy way to visually discern the buildup of debris. After the tool has been modified, cleaning is as simple as using two pins to push the debris out through the slots.

The second technique involves the use of air pressure to push out the trapped debris. The coring tool is removed from the drill and mounted on a pressure regulator. A vacuum hose is attached to the bottom of the drill to vent the debris safely into a receptacle.

This work was done by Joseph J. Gervais of Rockwell International for **Johnson Space Center**.
MSC-22672

Mathematics and Information Sciences

Hardware, Techniques, and Processes

Books and Reports

48

BLANK PAGE

Maximum-Likelihood Scheme for Tracking an Optical Source

Subpixel resolution should be possible, even in a high-disturbance environment.

NASA's Jet Propulsion Laboratory, Pasadena, California

A fine-pointing scheme that involves correlation of images and maximum-likelihood estimation has been proposed to enable tracking of optical sources. This scheme is intended for implementation in the pointing-control system of an imaging instrument (e.g., a telescope equipped with an image detector) to provide a capability for highly stable and accurate pointing to a specific area within a moving target, even under conditions that ordinarily give rise to pointing jitters. Such conditions include motion of the target relative to the instrument, instability of platform that supports the instrument-aiming mechanism, and turbulence in the atmosphere or other optical medium. In the original intended application, the scheme would be implemented in a ground station for tracking a laser that would be part of an optical communication aboard a distant spacecraft. Other potential applications include stabilization of images for video cameras and precise pointing of lasers in military, industrial, and surgical settings. This scheme is expected to make it possible to achieve subpixel resolution in a high-disturbance environment.

The scheme is based partly on the following assumptions:

- The image of the source occupies multiple pixels on the image detector. [For the purpose of this assumption, it does not matter whether (1) the source is larger than the equivalent of one pixel or (2) the source is smaller than the equivalent of one pixel but the image is smeared over more than one pixel because the telescope is intentionally defocused.]
- Data on a reference image of the source (e.g., a laser-intensity profile) are available for correlation with images on the detector.
- The spacecraft or other object to be tracked may be translating but is not rotating, relative to the tracking station.
- Differences or uncertainties between the reference image and the detected image at a given instant can be modeled as independent additive white Gaussian disturbances.

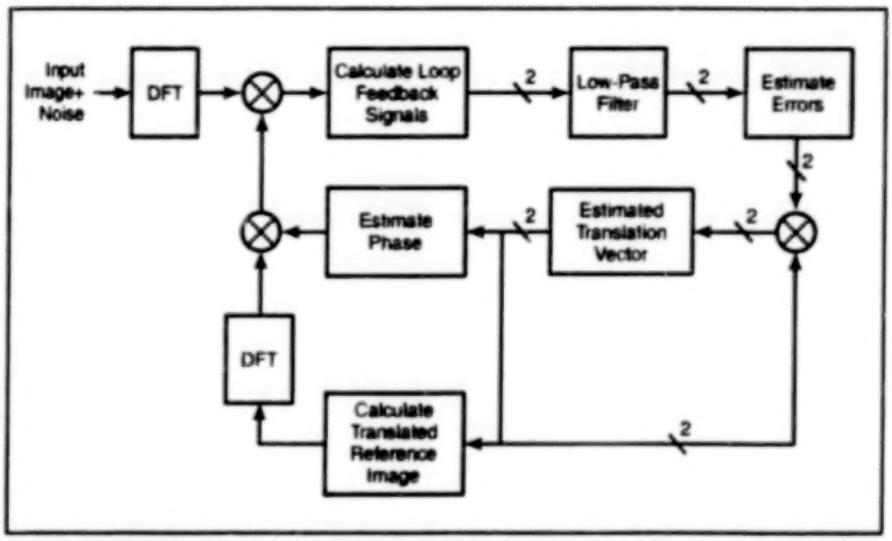

This Image-Tracking Loop would generate tracking signals from noise-corrupted, translating images of a source and a noiseless reference image of the source.

The proposed scheme utilizes discrete Fourier transforms (DFTs) of the image received at a sampling instant and of the reference image. Correlations between the received image and the original reference image are computed in the transform domain. The coordinates of the target in the image are estimated by an open-loop acquisition algorithm, then tracked by a closed-loop tracking algorithm. The open-loop acquisition algorithm involves the solution of two nonlinear equations that contain phase and amplitude correlation terms; the solution yields a maximum-likelihood estimate of the translation vector between the received and reference images.

The closed-loop tracking algorithm (see figure) also involves a maximum-likelihood estimation and the computation of weighted transform-domain correlations between received and reference images. However, instead of the original reference image, translated versions (based on estimates of translation) of the original reference image are used in these correlations. The loop feedback signals are low-pass filtered to obtain the current estimate of the error in the maximum-likelihood estimate of the translation vector. The closed-loop tracking algorithm also involves the solution of two nonlinear equations that involve phase and amplitude correlation terms, but assuming that phase errors remain small during tracking, these equations can be approximated closely by linear ones that yield error terms that can be used to update the maximum-likelihood estimates of the translation vector.

This work was done by Haiping Tsou and Tsun-Yee Yan of Caltech for **NASA's Jet Propulsion Laboratory**. *Further information is contained in a TSP [see page 1].*

This software is available for commercial licensing. Please contact Don Hart of the California Institute of Technology at (818) 393-3425. Refer to NPO-20698.

Quantum Superluminal Transmission of Random Messages

Messages that would not convey information could be useful for deception.

NASA's Jet Propulsion Laboratory, Pasadena, California

In a proposed communication scheme, quantum entanglement and quantum nonlocality would be utilized to effect instantaneous transmission of randomly chosen messages to remote locations. Although the messages would not convey any information, they might nevertheless be of some value under circumstances in which deception and secrecy are of more importance than are the specific contents of the messages.

The scheme would be implemented in

a simple quantum algorithm: The sender and recipient would each possess n particles, each of which could be in one of two equally probable quantum states denoted "+" and "–" (e.g., corresponding to spin up or spin down if the particles were electrons). Each particle at the sender's location would be paired with one of particles at the recipient's location by a quantum entanglement.

The sender and recipient would both perform a timed sequence of measurements on their particles — one particle per time step — so that at the end of n time steps, the sender and recipient would both possess n-length sequences of "+" and "–" readings. By performing the measurements, the sender would have randomly selected one of the 2^n possible sequences. The sequence would constitute a randomly chosen message. Because of quantum entanglement, the recipient's sequence would be uniquely correlated with the sender's sequence.

Given the randomness of the selection, the message would convey no information. The message may nevertheless have value under circumstances in which any of the 2^n possible messages would be equally effective in producing a desired outcome and there is a requirement to keep the message (that is, the randomly chosen sequence of "+" and "–") secret from everyone except the intended recipient. In such circumstances, the value would lie in secrecy and/or deception: the random selection would hide the actual message among 2^n–1 other messages.

This work was done by Michail Zak of Caltech for **NASA's Jet Propulsion Laboratory**. *Further information is contained in a TSP [see page 1].*
NPO-21036

Multirover Coordination Based on Contract Net Protocol

A computer program coordinates operations of multiple cooperating rovers (small exploratory robotic vehicles deployed from a lander spacecraft), each of which is equipped with computer hardware and software that schedule the tasks assigned to it. The program implements a contract net protocol — a type of coordination protocol commonly used in distributed artificial intelligence. In a contract net protocol, a manager announces a task to a set of contractors, each contractor bids for the task, and the manager awards the task to the contractor with the best bid. In the present program, the lander (manager) incrementally transmits tasks to each rover (contractor). Upon receiving a task, a rover tries to fit the task into its current schedule. If the rover can do so, it bids the total distance it would have to travel to complete all of its tasks (including the newly inserted one). Rovers that fail to fit the task into their schedules within a time limit do not participate in the auction. Upon receiving all bids, the lander awards the task to the rover with the smallest bid.

This program was written by Steve Chien, Gregg Rabideau, Tara Estlin, and Anthony Barrett of Caltech for **NASA's Jet Propulsion Laboratory**. *Further information is contained in a TSP [see page 1].*

This software is available for commercial licensing. Please contact Don Hart of the California Institute of Technology at (818) 393-3425. Refer to NPO-20940.

Books and Reports

Goal-Based Fault Tolerance for Spacecraft Systems

A report discusses the concept of goal-based fault tolerance as implemented in NASA's Mission Data System (MDS), which is a developmental architecture for unified flight, test, and ground software that is intended to be adaptable to a variety of next-generation deep-space missions. In goal-based fault tolerance, unlike in prior approaches to fault tolerance, it is not assumed that faults that necessitate deviations from prescribed sequences of commands will occur infrequently; instead, it is assumed that unpredictable conditions, including faults, can arise at any time, and fault tolerance is incorporated as an intrinsic feature of every aspect of system design in a unified approach to ensuring robust system behavior. Goal-based fault tolerance is a characteristic of goal-based closed-loop control, in which an autonomous system is designed to plan and execute its actions by reasoning in the light of the present state, in an attempt to satisfy goals prescribed by human operators (instead of following specific commands). "State" as used here denotes the collection of all relevant values (and their uncertainties) that characterize the environment and the physical condition and design of the system.

This work was done by Daniel Dvorak, Erann Gat, Kim Gostelow, Robert Rasmussen, and Steve Chien of Caltech for **NASA's Jet Propulsion Laboratory**. *To obtain a copy of the report, "Goal Based Fault Tolerance for Space Systems Using the Mission Data System," see TSP's [page 1].*

This software is available for commercial licensing. Please contact Don Hart of the California Institute of Technology at (818) 393-3425. Refer to NPO-21176.

Remote Agent as Applied to the Deep Space 1 Spacecraft

A report presents updated information about the Remote Agent — a reusable artificial-intelligence software system that was described in "A Remote Agent Prototype for Spacecraft Autonomy" (NPO-19992), *NASA Tech Briefs*, Vol. 21, No. 3 (March 1997), page 106. This system was conceived to enable spacecraft to operate robustly with minimal human supervision, even in the face of hardware failures or unexpected events. It also is expected to offer similar benefits for communication networks, chemical plants, and other complex systems on Earth. The report summarizes the functionality and structure of the Remote Agent and discusses the application of the innovative Remote Agent artificial intelligence system to control of the Deep Space One (DS1) Spacecraft, which is used as an innovative artificial-intelligence system to control a spacecraft. In a series of experiments, the Remote Agent (1) planned its own mission activities on the basis of mission goals provided by human operators and (2) carried out its plan by commanding the spacecraft. The experiments included diagnosis of an onboard failure and response by replanning part of the mission to ensure that mission goals were achieved.

This work was done by Douglas Bernard; Edward Gamble, Jr.; Benjamin Smith; Nicolas Rouquette; Erann Gat; Yu-Wen

Tung; Guy Man; Robert Rasmussen; Steve Chien; Scott Davies; Daniel Dvorak; Greg Rabideau; and David Yan of **NASA's Jet Propulsion Laboratory**; *P. Pandurang Nayak, Bob Kanefsky, James Kurien, William Millar, Kanna Rajan, Brian Williams, Charles Fry, Gregory Dorais, Barney Pell, Ronald Keesing, Christian Plaunt, William Taylor, Scott Sawyer, Greg Swietek, Greg Whelan, Sunil Mohan, Paul Morris, and Mike Wagner of Ames Research Center; and Reid Simmons of CMU. To obtain a copy of the report, "Remote Agent, autonomous reasoning and control for spacecraft and other complex systems," see TSP's [page 1].*

This software is available for commercial licensing. Please contact Don Hart of the California Institute of Technology at (818) 393-3425. Refer to NPO-20867.

BLANK PAGE

Life Sciences

Hardware, Techniques, and Processes

54

BLANK PAGE

Advanced System for Growing Plants in Microgravity

Plants can be observed during growth under controlled conditions.

John F. Kennedy Space Center, Florida

The figure depicts the Biomass Production System (BPS), which is an advanced system that provides controlled conditions for growing, manipulating, sampling, and harvesting plants in microgravity for both commercial purposes and scientific research. The design of the BPS incorporates lessons learned from the operation of prior plant-growth systems aboard spacecraft in flight. Examples of uses for the BPS include (1) metabolic experiments that can include photosynthesis, respiration, and transpiration; (2) biotechnological plant investigations; and (3) side-by-side comparison of multiple plant-growth techniques and conditions. Plant biomass is easily accessible during all phases of operation.

The subsystems of the BPS feature modular designs. The BPS currently includes four plant-growth chambers with independent monitoring and control of temperature, humidity, lighting, the concentration of CO_2 for each chamber, and nutrient delivery. The chambers are sealed for gas-exchange measurements, and there are multiple gas/liquid-sampling ports. By modifying the design, the chamber configuration can be changed from four independent chambers to two tall, two wide, or one large chamber.

The overall operation of the BPS is coordinated by an advanced electronic control and monitoring subsystem with a capability for automated diagnosis. Features of this subsystem include one video camera (with expansion capabilities to two cameras) in each chamber for observation in real time, a fully equipped computer with a serial port and an Ethernet interface for direct transfer of data, enhanced capabilities for acquisition and storage of data (including image data), fuzzy logic for control of temperature and humidity, front-panel controls with full command authority, a high-resolution color front-panel display, indicators of operational status, an interface key pad, a standard floppy-disk drive, a standard keyboard interface, programmability of data-handling functions, and menu-driven software with optional displays defined by the user.

The BPS includes modular lighting and active metered nutrient-delivery subsystems that can be controlled separately or together. The temperature-control subsystem includes a high-performance thermoelectric controller. The lighting-control subsystem includes an efficient solid-state ballast light-controller/driver circuit. Other subsystems include a replenishable CO_2 supply, a regenerative H_2O-recovery loop, and a replenishable H_2O supply.

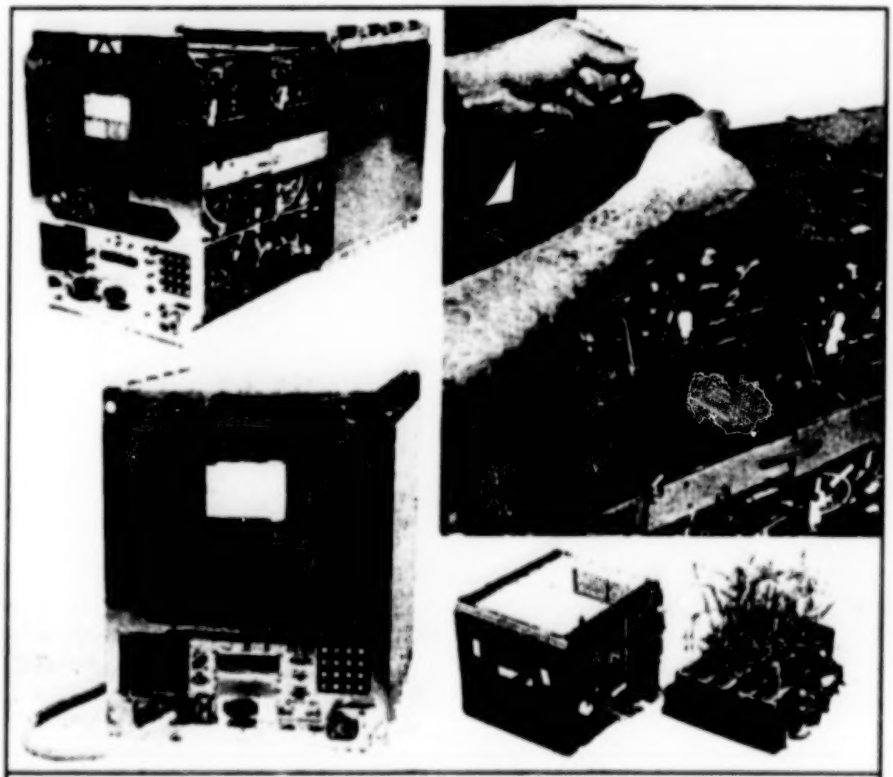

ENGINEERING SPECIFICATIONS

Temperature:	18 to 35 °C
Relative Humidity:	60 to 90%
Light Level:	50 to 375 μmole $m^{-2}s^{-1}$ (Baseline — Cool White Flouresoent Lamps)
CO_2 Monitoring and Enrichment:	Up to 10,000 Parts per Million
Capacity for Supply and Collection of Water:	Two Reservoirs Totaling 1,300 mL
Numbers and Size of Plant-Growth Chambers:	
Four Chambers	Each 16.5 × 14.6 × 18.8 cm
Two Tall Chambers	Each 16.5 × 14.6 × 40.4 cm
Two Wide Chambers	Each 16.5 × 37.5 × 18.8 cm
One Large Chamber	16.5 × 37.5 × 40.4 cm

The Biomass Production System is a modular system that provides controlled conditions for growing plants in microgravity.

This work during the SBIR Phase I and Phase II efforts included contributions from Ronald J. Anderson, Thomas M. Crabb, John G. Frank, Steven M. Guetschow, Jeffrey T. Iverson, Olaf Meding, Robert C. Morrow, E. Don Peissig, Ross W. Remiker, Robert C. Richter, David Smith, Jon D. Van Roo, Anton G. Vermaak, and John C. Vignali of Orbital Technologies Corp. for **Kennedy Space Center**.

KSC-12042

X-Ray Measurement of Kinematics in Muscles and Limbs

Positions and velocities of hundreds of implanted targets could be measured simultaneously.

NASA's Jet Propulsion Laboratory, Pasadena, California

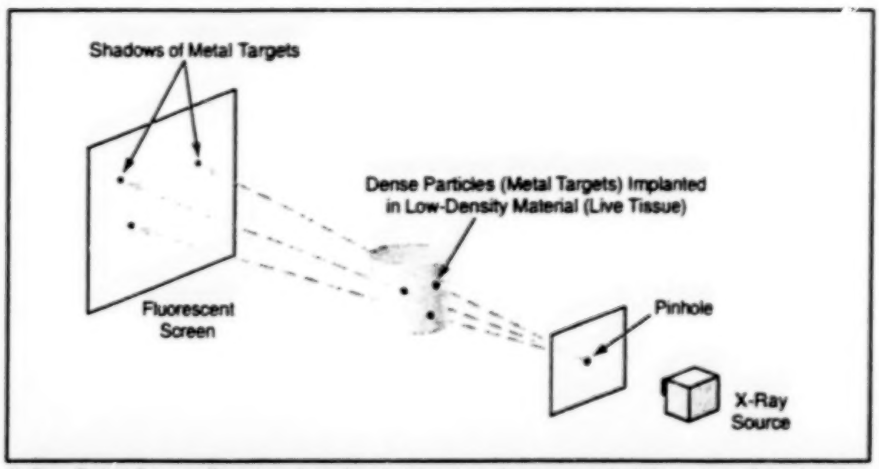

X-Ray Point-Source/Shadow Imaging is based on the same principle as that of the familiar visible-light pinhole camera. In this case, microscopic implanted metal targets would give rise to high-contrast spot shadows in the x-ray image.

An x-ray photogrammetric technique for minimally invasive measurement of displacements in muscles, limbs, and organs is undergoing development. This technique could be alternative or complementary to the use of strain sensors. Measurements obtained by this technique could also be compared directly with both absolute and differential measurements of muscle and skeleton kinematics obtained by exoskeletal devices or from video images of external motion.

The technique is based on x-ray point-source/shadow imaging of small implanted biocompatible metal targets (see figure). The dimensions of the targets would be much smaller than those of the body parts into which they would be inserted; e.g., a target for implantation in a 50-μm-diameter muscle fiber would have a diameter of about 5 μm. The targets would be implanted by use of a hypodermic needle. The targets would show up as dark spots in an x-ray image, which would be projected onto a fluorescent screen monitored by a video camera. A complete imaging system would include at least two (and preferably three) point-source/fluorescent-screen/video-camera assemblies oriented along different coordinate axes, plus frame grabbers, video image digitizers, and an image-data-processing computer.

Individual targets would be identified and their three-dimensional positions computed from the positions of their shadow spots in the x-ray images. With sufficiently fast frame grabbers and sufficient computing capacity, it would be possible to compute the coordinates of hundreds of targets at video frame rates. Velocities and accelerations of targets could readily be computed from changes in their positions in successive frames. Combining the results of these computations with knowledge of which particle is embedded in which tissue, one could establish the kinematics of the entire organism or body part in which the ensemble of targets was embedded. Inasmuch as gray-scale x-ray images generally show such tissues as bones and dense muscles, the information thus generated could be processed further to obtain enhanced animated images of body parts in motion. The original intended application for this technique is monitoring of fibrillation or operation of heart valves. Other potential applications include monitoring fatigue or cramps in muscles or acquiring data for calibration of mathematical models of muscle and limb movements and of muscle forces and displacements.

This work was done by Frank Hartley of Caltech for **NASA's Jet Propulsion Laboratory**. *Further information is contained in a TSP [see page 1].*

NPO-20467

END

04-30-02